Inexpensive 2D Optical Sensor for GPS Augmentation

Final Report

Prepared by:

Pi-Meng Cheng
Craig Shankwitz
Eddie Arpin

Intelligent Vehicles Laboratory
Department of Mechanical Engineering
University of Minnesota

CTS 12-37

Technical Report Documentation Page

1. Report No. CTS 12-37	2.	3. Recipients Accession No.	
4. Title and Subtitle Inexpensive 2D Optical Sensor for GPS Augmentation		5. Report Date December 2012 6.	
7. Author(s) Pi-Ming Cheng, Craig Shankwitz, and Eddie Arpin		8. Performing Organization Report No.	
9. Performing Organization Name and Address Department of Mechanical Engineering University of Minnesota 500 Pillsbury Drive SE Minneapolis, MN 55455		10. Project/Task/Work Unit No. CTS Project #2010073 11. Contract (C) or Grant (G) No.	
12. Sponsoring Organization Name and Address Intelligent Transportation Systems Institute Center for Transportation Studies University of Minnesota 200 Transportation and Safety Building 511 Washington Ave. SE Minneapolis, MN 55455		13. Type of Report and Period Covered Final Report 14. Sponsoring Agency Code	
15. Supplementary Notes http://www.its.umn.edu/Publications/ResearchReports/			

16. Abstract (Limit: 250 words)

Differential Global Positioning Systems (DGPS) are susceptible to outages due to blocked or missing satellite signals and/or blocked or missing DGPS correction messages. Outages arise primarily due to environmental reasons: passing under bridges, passing under overhead highway signs, adjacent foliage, etc. Generally, these outages are spatially deterministic, and can be accurately predicted. These outages distract drivers using DGPS-based driver assistive systems, and limit the system robustness. Inertial measurements have been proposed as an augmentation for DGPS. Tests have shown that error rates for even emerging technologies are still too high; a vehicle can maintain lane position for less than three to four seconds. Ring laser gyros can do the job, but $100K per axis is still too expensive for road-going vehicles. To provide robust vehicle positioning in the face of DGPS outages, the IV Lab has developed a technique by which a non-contact, 2D true ground velocity sensor is used to guide the vehicle. Although far from fully developed, the system can maintain vehicle position within a lane for GPS outages of up to 20 seconds. New dual frequency, carrier phase DGPS systems generally require less than 20 seconds to acquire a "fix" solution after a GPS outage, so the performance of this system should be adequate for augmentation. Proposed herein is basic research which may lead to the development of an inexpensive, 2D, non-contact velocity sensor optimized for vehicle guidance during periods of DGPS outages.

17. Document Analysis/Descriptors Differential Global Positioning System, Global Positioning System, System robustness, Driver support systems, GPS augmentation		18. Availability Statement No restrictions. Document available from: National Technical Information Services, Alexandria, Virginia 22312	
19. Security Class (this report) Unclassified	20. Security Class (this page) Unclassified	21. No. of Pages 79	22. Price

Inexpensive 2D Optical Sensor for GPS Augmentation

Final Report

Prepared by:

Pi-Ming Cheng
Craig Shankwitz
Eddie Arpin

Intelligent Vehicles Laboratory
Department of Mechanical Engineering
University of Minnesota

December 2012

Published by:

Intelligent Transportation Systems Institute
Center for Transportation Studies
University of Minnesota
200 Transportation and Safety Building
511 Washington Avenue SE
Minneapolis, Minnesota 55455

Acknowledgments

The authors wish to acknowledge those who made this research possible. The study was funded by the Intelligent Transportation Systems (ITS) Institute, a program of the University of Minnesota's Center for Transportation Studies (CTS). Financial support was provided by the United States Department of Transportation's Research and Innovative Technologies Administration (RITA).

Table of Contents

Appendix A: Results of Constant Speed, Constant Angle Tests

Appendix B: Angular Measurements of ADNS-3080 Sensor

Appendix C: Results of Linear Speed Tests of ADNS-3080 Sensor

Appendix D: Results of Angle Measurements at Different Moving Roadway Speeds

Appendix E: Results of Angle Measurements at 1º Increment and Different Data Output Rate

Appendix F: Results of Angle Measurements at 4" above the Moving Roadway

Appendix G: Results of Angle Measurements at 1600 cpi Sensor Resolution

Appendix H: Results of Angle Measurements at 1600 cpi Sensor Resolution, Height at 9"

Appendix I: Results of Angle Measurements at 1600 cpi Sensor Resolution, Height at 9" with 25 mm Lens

Appendix J: Results of Angle Measurements at 1600 cpi Sensor Resolution, Height at 4" with 17 mm Lens

Appendix K: Results of Angle Measurements at 1600 cpi Sensor Resolution, Height at 6" with 25 mm Lens

List of Figures

List of Tables

Executive Summary

Background

The Intelligent Vehicles Lab (IV Lab) at the University of Minnesota has been developing GPS-based driver assistive technologies for more than 15 years. These Driver Assistive Systems (DAS) can help drivers navigate through difficult weather and traffic conditions. The system has been deployed in several locations in Minnesota and Alaska. Under U.S. DOT's Urban Partnership Agreement (UPA), 10 transit buses in the Twin Cities metro area were equipped with DAS. Since these 10 buses are operated in an urban environment, an augmentation system was developed to help DAS guide a vehicle during GPS outages when it travels under bridges, overhead signs, etc. The augmentation system is based on a commercial-off-the-shelf 2D optical velocity sensor used to measure vehicle velocities with respect to the ground. The results were good and the augmentation system has been working for more than 2 years. However, each optical velocity sensor costs around $20,000. The goal of this proof-of-concept research is to develop an inexpensive alternative sensor that can eventually be used in the augmentation system to guide a vehicle when GPS signals are not available.

Objectives

The main objective of this study is to develop an inexpensive 2D velocity sensor for GPS augmentation applications. The sensor should be able to measure vehicle velocities with respect to the ground consistently and reliably.

Key Findings

Several different technologies were researched and an optical mouse sensor that can do image-based motion estimation based on the theory of optical flow was selected as the alternative inexpensive speed sensor. A sensor based on the Avago ADNS-3080 mouse sensor chip with modified optics was constructed and evaluated both in the lab on a simulated moving roadway and in the field on real roads.

The main results of the evaluations are listed as follows:

- ADNS-3080 mouse sensor can measure speed up to 48 MPH (21.5 m/sec) and angles all around from 0° to 360°.
- Speed output of the ADNS-3080 mouse sensor was linearly proportional to the actual speed measured. The coefficient of determination (R^2) in the linear regression analysis was close to 1 for both in-lab testing and on-road evaluation.
- There exist deadbands for the ADNS-3080 mouse sensor near the X (horizontal) and Y (vertical) axes. To avoid deadbands, the sensor was physically rotated 45° in the sensor box before mounting on a vehicle.
- Excluding deadbands, in-lab testing showed that the ADNS-3080 mouse sensor had a mean angular measurement error of 1.245° with a standard deviation of 1.418° when the resolution was configured to 400 cpi and the mouse sensor was placed at 9" (229 mm) above the "road" surface. The standard deviation decreased when the resolution

of the sensor was set at 1600 cpi. It had a mean angle error of 1.575° with a standard deviation of 0.236°.

- Performance did improve when the ADNS-3080 mouse sensor was placed at 4" (102 mm) above the road surface. However, the sensor and/or the illumination lamp could easily suffer damages if they were located too close to the ground in a real life situation. Therefore, it was decided that the sensor should be mounted at 9" (229 mm) above the ground on a vehicle in the field evaluation.
- Performance of ADNS-3080 mouse sensor in the field was not as consistent as performance observed in the lab. In speed analysis, the coefficient of determination (R^2) was lower. In angle analysis, both the mean angle measurement error and variance were larger.

The ADNS-3080 mouse sensor showed promising results that it has the potential to replace the more expensive optical speed sensor currently used on UPA buses. However, more research is needed to improve the performance of the sensor in the field on real roads.

Chapter 1. Introduction

1.1 Background

In urban and suburban environments, GPS outage is a common problem in GPS-based vehicle guidance applications. A GPS outage can be attributed to driving in downtown through a series of tall buildings, passing under bridges, overhead signs, etc. An outage can last from seconds to minutes. In the U.S. DOT's Urban Partnership Agreement (UPA) project, the Intelligent Vehicles Lab (IV Lab) developed a vehicle-based GPS augmentation system (VBAS) to guide a vehicle when GPS signals are lost. The VBAS system is based on a commercial-off-the-shelf 2-D optical velocity sensor, Correvit S-350, to measure 2D ground velocities and heading angles. The system demonstrated a less than 3.94" (10 cm) lateral positional error after a bus driving under an overpass bridge [1].

1.2 Correvit S-350 Sensor

The Correvit S-350 Aqua sensor is manufactured by Corrsys Datron [2]. It is a 2-axis non-contact optical velocity sensor. It measures velocity between the sensor and the road surface and uses a halogen lamp to illuminate the roadway surface in the field of view of the sensor. Figure 1.1 shows a S-350 sensor and Table 1.1 shows the specifications of the sensor.

Figure 1.1 Correvit S-350 Aqua speed sensor.

1.3 Correvit Sensor Performance

The Correvit speed sensor has been in service on UPA buses since 2009. In-lab testing showed that the sensor was accurate to within 0.1 m/sec (with a standard deviation of 0.164 m/sec) on speed measurements [3]. On angle measurements, the sensor had a mean error of 0.747° (with a standard deviation of 1.084°) [3]. The Correvit sensor is very durable and has had a zero failure rate since 10 of them were installed and put in service on UPA buses in 2009.

1.4 Project Goal: Inexpensive 2-D Speed Sensor

The Correvit S-350 speed sensor can provide accurate measurements of vehicle velocities and slip angles. However, each unit costs around $20,000. This study is aimed at developing a sensor which is relatively inexpensive compared to the Correvit sensor and is still able to be used in the VBAS system to measure vehicle velocities to augment GPS vehicle guidance in the event that GPS signals are lost.

Table 1.1 Performance specifications of Correvit S-350 Aqua speed sensor.

Parameter	Unit of measure	value
Update Rate	Hertz	250
Speed Range	km/h	0.5 – 250
Distance Resolution	mm	2.47
Distance Measurement Accuracy	%	< +/- 0.2
Velocity Resolution	m/s	0.6175
Velocity Measurement Accuracy	%	< +/- 0.2
Angle Range	Degrees	+/- 40
Angle Resolution	Degrees	< +/- 0.1
Angle Measurement Accuracy	Degrees	< +/- 0.2
Working range	mm	350 +/- 100

1.5 Literature Review

Inertial navigation system has been used in aircraft, guided missiles, and spacecraft for decades [4]. Recent developments on inertial measurement units (IMUs) allow IMUs to be integrated into GPS-based vehicle guidance systems. IMUs allow the guidance system continue to function when GPS signals are not available. In a vehicle guidance system, IMUs measure accelerations and rotational rates. Using initial conditions, equations of motion are integrated to produce estimates of vehicle position, velocity, and orientation.

IMU suffers from integration drift associated with the bias from accelerometers and rotational rate sensors. The small bias error in acceleration can soon be compound into a large positional error, resulting in an "out of lane" condition within several seconds.

Image based motion detection based on the theory of optical flow has been developed since 1940s [5]. It is used by robotics researchers to do object detection and tracking. By comparing a sequence of ordered images, one can compute motion (i.e., displacement and velocity) of an object in the image frames.

Figure 1.2 shows an object moving toward bottom right (in the field of view) in two consecutive image frames from time t to $t+\Delta t$. By comparing sequence of images, motion detection algorithms can determine the direction that the object is moving between adjacent frames and compute vectors describing that relative motion [6].

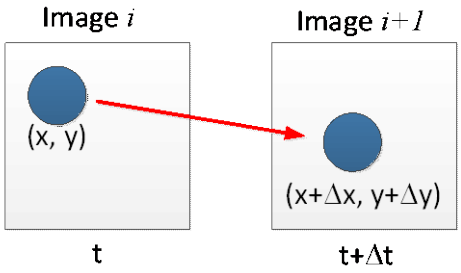

Figure 1.2 Motion of an object from time t to $t+\Delta t$ in consecutive images.

Since 1980s, this technique has been applied to input pointing devices (i.e., computer mice) for computers [7]. Today, an optical mouse is capable of capturing thousands of successive images

per second. By comparing overlapping parts of sequential images, an optical mouse can calculate relative movement with corresponding Δx and Δy values. These values are stored in registers and are accessible by a host computer or microcontroller to translate the movement of an optical mouse to the movement of cursor on the computer screen.

The use of optical mouse sensor as a low-cost 2D velocity sensor has been mentioned in several studies. In [8], an optical mouse sensor was used to estimate the motion of a robot in a rough terrain environment under low speed (< 0.62 ft/sec or 0.19 m/sec). In [9], the sensor was used as a speedometer on a skateboard. The results showed that the sensor can measure speed up to 20 MPH (8.9 m/sec) with an error up to 10% of the measured speed. In [10], two optical mouse sensors were used to measure the velocity and yaw rate of a moving vehicle. Their results showed non-linearity in velocity measurement and about 6°/sec of error in yaw rate measurement in experimental runs. In [11], an optical mouse sensor was fitted to do positional control of a flying model helicopter. Since the camera lens used in an optical mouse sensor is designed to focus on the surface only few millimeters below the sensor, the optical imaging system needs to be modified with a different lens for each application in order to create focused images on the sensor.

1.6 Selection of Optical Mouse Sensor

Several different factors need to be considered before selecting an optical mouse sensor for this study. These factors include frame rate, image size, resolution, and cost.

Frame Rate

The frame rate is the number of images that an optical mouse sensor can take per second. For a given image sensor, one with a higher frame rate indicates its ability to detect a small movement, therefore, capable of tracking at higher speeds. An optical mouse sensor usually has a programmable frame rate between 500 frames per second (fps) to more than 6400 fps.

Image Size

A typical optical mouse sensor uses an imaging sensor with 18×18 pixels. A high performance mouse sensor has a 30×30 pixel imaging sensor. If two sensors are configured to run at the same frame rate, the 30×30 pixel sensor is capable of providing a larger image and be able to track at a higher speed than the 18×18 pixel sensor.

Resolution

Resolution of an optical mouse sensor indicates the level of surface details that can be captured by the sensor. Mice used for office applications usually have a lower resolution of 400 counts per inch (cpi). A higher resolution of 1600 cpi is usually desired in applications where measurements of fast and accurate movements are required (i.e., gaming applications). In this study, it was found that a more sensitive sensor (at 1600 cpi) would be helpful to detect more detailed surface texture especially when the distance between the sensor and the road surface was increased.

Cost

As optical mice became popular and mainstream, the cost of sensor chips decreased. A raw sensor chip can be ordered from an internet retail store for less than $5 [12]. An integrated optical mouse sensor breakout board with a camera lens mount and communication interface can be purchased for $40 [13]. To speed up the development process and prevent circuit design errors, integrated optical mouse sensor breakout boards were used in this study.

Avago Technologies provides the most comprehensive array of optical mouse sensors. Table 1.2 compares features of several such sensors [14]. From the list, it was determined that ADNS-3080, a high performance gaming mouse sensor that is capable of accurately tracking fast motion, would be used in this study.

Table 1.2 Comparison of optical mouse sensors.

Sensor		**ADNS-2610**	**ADNS-2051**	**ADNS-3080**
Feature	Units	Entry level	Mid range	High performance
Image size	pixels	18x18	18x18	30x30
Frame rate	fps	1500	500 ~ 2300	500 ~ 6469
Resolution	cpi	400	400/800	400/1600

1.7 Optical Property

The integrated ADNS-3080 breakout board comes with a M12x0.5 pitch lens mount. The system can be paired with different focal length of lenses if desired. To achieve a clear and focused image, the following equation is used to calculate the required focal length *f* of a lens (Figure 1.3):

$$\frac{1}{f} = \frac{1}{r_1} + \frac{1}{r_2}$$

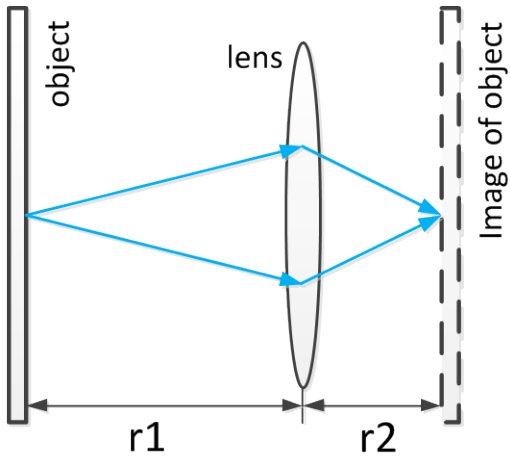

Figure 1.3 Optical property of lens.

However, in reality, M12 lenses can only be purchased with certain stock sizes of focal lengths. Furthermore, since the sensor is going to be used as a 2D speed sensor on a moving vehicle, r_1 should not be less than 9" (229 mm) from the road surface (to prevent the sensor from hitting the ground). The above equation can be used as a guideline to adjust and fine-tune the distance between the lens and the ADNS-3080 sensor (r_2). More details will be discussed in Chapter 2, including image sizes of different lenses and effects of speeds on overlaps of consecutive image frames.

In this study, several lenses with different focal lengths were tested. Distances between the lens and the road surface were also varied in lab testing to compare results and test the sensitivity of the ADNS-3080 sensor. More detailed are discussed in Chapter 2.

Chapter 2. In-Lab Evaluation of ADNS-3080 Sensor

2.1 ADNS-3080 Mouse Sensor

The Avago ADNS-3080 was selected as the mouse sensor to be evaluated. Key features of the sensor include:

- Large image size of 30 x 30 pixels;
- Programmable frame rate from 500 to 6469 frames per second (fps);
- Either self-adjusting or manual frame rate and shutter speed;
- Burst mode for fast data transfer;
- Adjustable resolution either 400 or 1600 cpi;
- Four-wire Serial Peripheral Interface Bus (SPI) port for data communication.

According to the specification sheet, additional circuits including resonator, voltage regulator and power control need to be implemented for the ADNS-3080 chip to function. To speed up the development process, an integrated ADNS-3080 breakout board (Figure 2.1) was purchased from the DIY Drone store [13].

Figure 2.1 Integrated ADNS-3080 breakout board (dimensions: 33x25 mm).

The integrated ADNS-3080 board has all the necessary circuits and can be interfaced directly with a microcontroller. The breakout board also includes a M12x0.5 lens mount and the lens can be easily changed if required.

2.2 mbed Microcontroller

The mbed NXP LPC1768 microcontroller (Figure 2.2) is a single board microcontroller. It is based on an ARM Cortex M3 processor and runs at 96 MHz. The microcontroller has 512 KB of flash, 32 KB of RAM, and analog and digital input/output ports. It also has several communication interfaces including Ethernet, USB, CAN, SPI, and I^2C.

An on-line compiler is used to generate program binaries. A C/C++ SDK is available to allow high-level programming of peripherals. Once a program binary is generated, the built-in USB drag ‘n’ drop interface is used to upload the binary code to the microcontroller. Figure 2.3 shows a NXP LPC1768 microcontroller on a baseboard interfaced with an integrated ADNS-3080 breakout board.

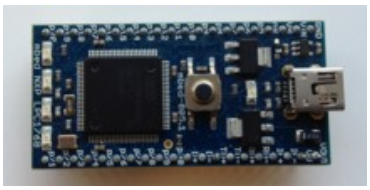

Figure 2.2 mbed NXP LPC1768 microcontroller (dimensions: 54x26 mm).

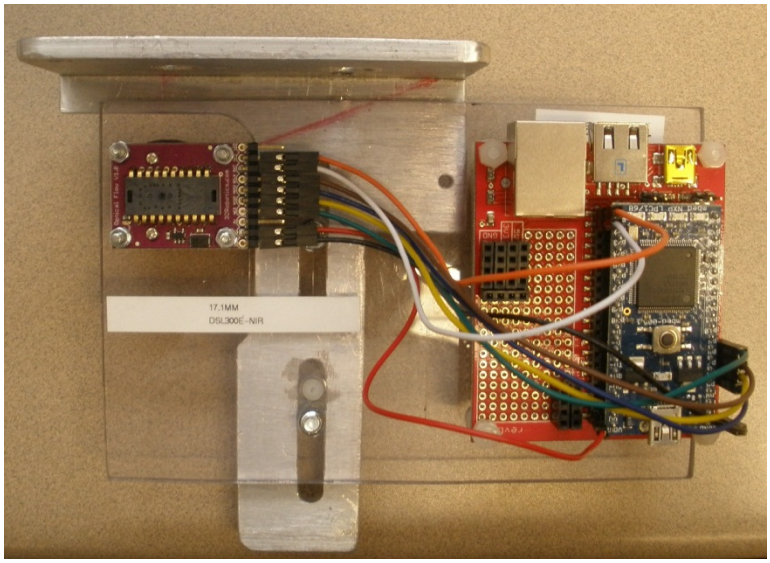

Figure 2.3 mbed NXP LPC1768 microcontroller interfaced with an ADNS-3080 sensor board.

In this project, the mbed microcontroller is used as a conduit between the host computer and the ADNS-3080 sensor. It has direct access to all data registers on the ADNS-3080 sensor. The microcontroller initializes, configures and reads motion data from registers on the ADNS-3080 sensor and then send data out to a host computer via Ethernet. The mbed microcontroller board also provides power to the ADNS-3080 sensor.

Figure 2.4 shows a flowchart of the communication process. The ADNS-3080 sensor has an internal buffer that can cache motion data internally. The mbed microcontroller is programmed to read motion data from the ADNS-3080 sensor every 200 μsec (i.e., 5000 Hz), and compute and accumulate overall motion data in its memory. It then sends data to the host computer and reset the memory for motion data every 10 msec (i.e., 100 Hz). Please note that the ADNS-3080 sensor does not have much internal memory buffer. Therefore, the microcontroller needs to read data fast enough before the ADNS-3080 internal buffer overflows.

As a part of the communication protocol, the ADNS-3080 sensor also outputs surface quality readings, which indicate the number of features that the sensor can pick up from the surface. A high surface quality number (usually greater than 100) shows that the sensor can pick up large number of surface details, which can enhance its ability to track reliably.

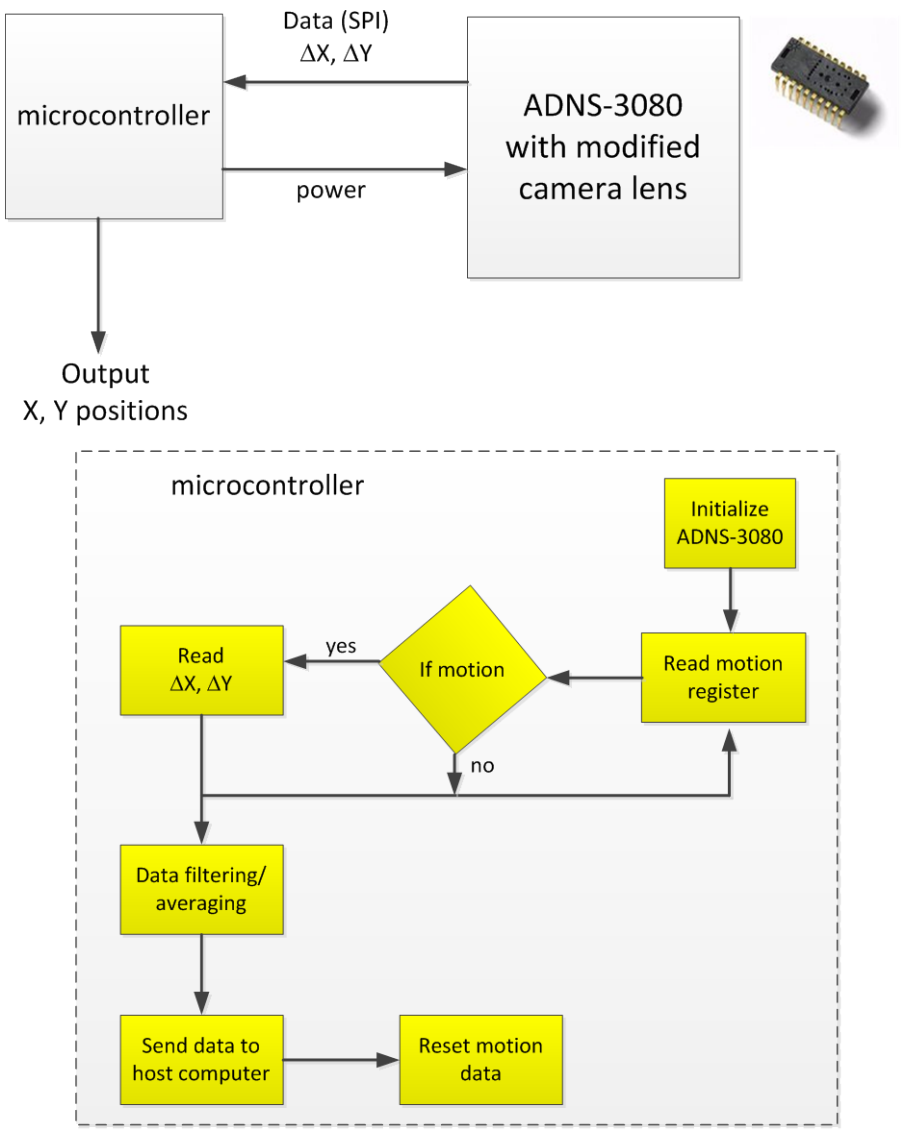

Figure 2.4 Flowchart of communication between the microcontroller and the ADNS-3080 sensor.

2.3 Testbed

A testbed, which simulates a moving roadway, is used to evaluate the ADNS-3080 mouse sensor in the lab. Figure 2.5 shows the setup. The testbed is based on a rock tumbler with a Baldor ¼ horsepower DC motor. The motor is controlled by a Baldor BC-141 SIH controller board. The controller has analog voltage input ports, which allows direct control of motor speed from a host computer. The DC motor drives rotating shafts and two pulleys with a belt connecting between the two pulleys. The pulleys have a diameter of 4.63" (117.5 mm) and the motor can spin up to 5000 rpm, thus providing a simulated roadway with speed up to 69 MPH (31 m/sec).

In an optical mouse, a light-emitting diode (LED) is used as a light source to illuminate the surface underneath the mouse. The light source creates highlights and shadows on the surface to

allow the camera to pick up detailed surface texture. A Philips halogen light bulb with aluminum reflector is used in the testbed as a light source (F in Figure 2.5). After adjustment, the mouse sensor produces high surface quality readings, an indication that the sensor picks up large numbers of features from the surface and tracks reliably.

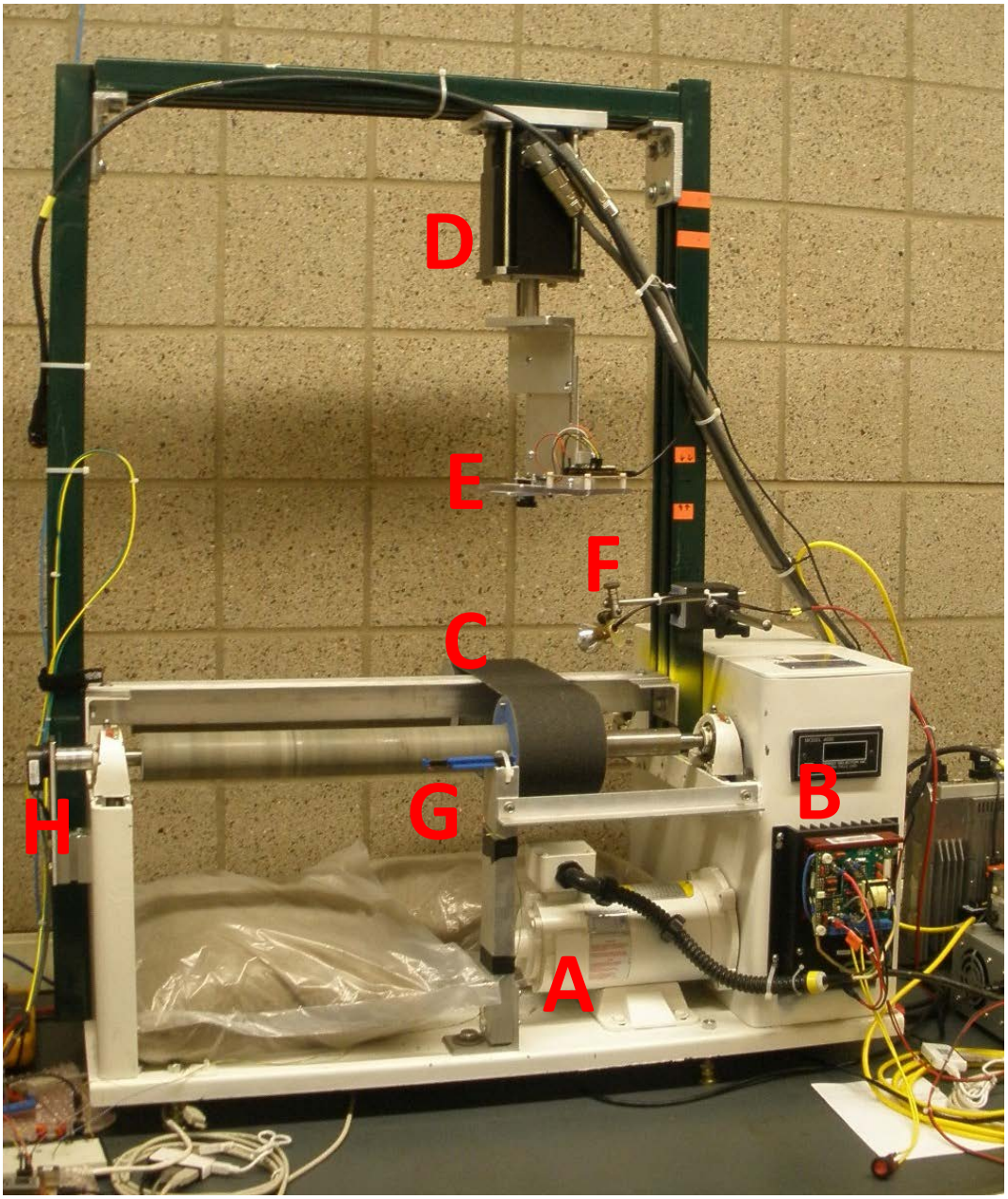

Figure 2.5 ADNS-3080 sensor testbed (where A: DC motor, B: motor controller, C: moving roadway, D: servo motor, E: ADNS-3080 sensor, F: illumination light source, G: magnetic pickup speed sensor, H: optical encoder speed sensor).

The speed of the simulated roadway (i.e., belt) can be measured in two ways. The first method is to use an embedded magnet in the front pulley and a magnetic pickup circuit (G in Figure 2.5). When the roadway moves, the magnetic pickup would generate a voltage whenever the

embedded magnet passes through. The time, *T*, between two rotations (i.e., two voltage pulses) is measured by a microcontroller and the speed of the simulated roadway can be calculated using:

$$S_{ROAD} = \frac{\pi D}{T}$$

where *D* is the diameter of the pulley (4.63", or 117.5 mm).

The second method is to use an encoder connected to a rotating shaft (H in Figure 2.5). The encoder is a US Digital H15 single-ended encoder with 360 counts per revolution. The speed of the simulated roadway can be calculated by measuring the encoder counts for a specific time period. This is a more accurate way of measuring the speed of the simulated roadway as the encoder provides 360 counts per revolution while the magnetic pickup circuit only provides one count per revolution. Currently, a microcontroller is programmed to read the encoder every 20 msec (50 Hz), and the speed of the simulated roadway can be calculated using:

$$R = \left(\frac{counts}{360} \right) \Big/ dt$$
$$S_{ROAD} = \pi D \times R$$

where *R* is revolutions per second, *dt* is 20 msec, and *D* is the diameter of the pulley (4.63" or 117.5 mm).

In addition to the moving roadway, the mouse sensor is mounted on a servo motor, which rotates the sensor with respect to the moving roadway to simulate a vehicle slip angle. Together with the moving roadway, the mouse sensor can be evaluated at different slip angles and different roadway speeds. The slip angles are controlled by a 1,000,000 counts per revolution encoder embedded inside the servo motor. This 1,000,000 counts per revolution encoder provides a 0.00036° resolution and is used as a reference to compare against angle measurements made by the ADNS-3080 mouse sensor.

2.4 Image Calibration

The lens and LED light source that are included in the ADNS-3080 kit are designed to allow the ADNS-3080 sensor to detect and measure motion 0.08" (2 mm) above the surface. However, in this project, the ADNS-3080 sensor is to be used as a speed sensor on a vehicle. Therefore, the optic component of the sensor needs to be modified and calibrated in order for the ADNS-3080 sensor to function correctly at the desired height above the roadway.

Figure 2.6 shows three different settings that were used on the testbed to evaluate the ADNS-3080 mouse sensor. To achieve good surface quality numbers (i.e., high quality focused images), a light source (F in Figure 2.5) is used to illuminate the roadway surface. Figure 2.6 (A) shows a raw image dump of the ADNS-3080 sensor with a Sunex DSL300 17 mm lens. After adjusting the focal length, the sensor can detect an area of 0.39" × 0.39" (9.9 × 9.9 mm) at 4" (102 mm) above the roadway surface. This is equivalent to a 0.013" × 0.013" (0.33 × 0.33 mm) per pixel resolution. Figure 2.6 (B) shows an image snapshot of the ADNS-3080 sensor with a 25 mm lens from Edmund Optics and the sensor can detect an area of 0.51" × 0.51" (12.9 × 12.9 mm) at 9"

(229 mm) above the roadway with a 0.017” × 0.017” (0.43 × 0.43 mm) per pixel resolution. Figure 2.6 (C) shows an image captured by the ADNS-3080 sensor with a Sunex DSL300 17 mm lens and a detected area of 0.75” × 0.75” (19 × 19 mm) at 9” (229 mm) above the surface with a 0.025” × 0.025” (0.64 × 0.64 mm) per pixel resolution.

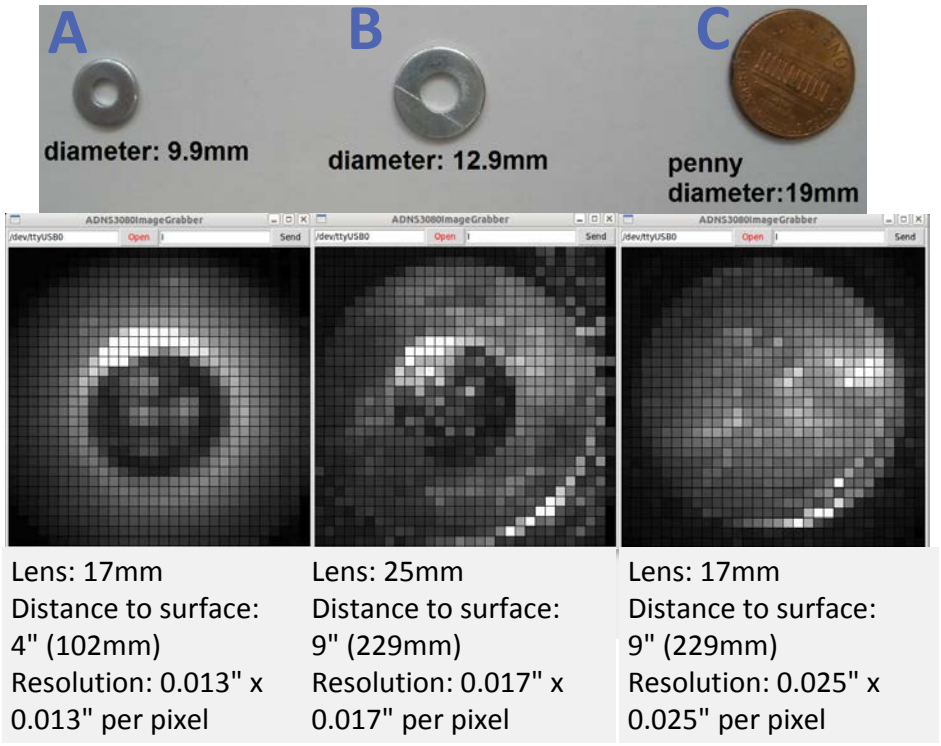

Figure 2.6 Raw images from ADNS-3080 sensor.

Assuming that the moving roadway is running at 48 MPH (21.5 m/sec), configuration shown in Figure 2.6(a) has a 66% overlap between consecutive image frames. Configurations in Figure 2.6(b), and (c) have a 74%, and 82% overlap between consecutive frames, respectively. At 48 MPH (21.5 m/sec), all three configurations meet the requirement of 65% overlap between consecutive frames for tracking [10]. With a 17 mm lens at 9” (229 mm) above the moving roadway (Figure 2.6(c)), the ADNS-3080 sensor can theoretically track up to 95 MPH (42.46 m/sec).

2.5 Experimental Design

The performance of the ADNS-3080 mouse sensor was measured at various moving roadway speeds and different slip angles to evaluate sensor measurement error. Tests were conducted with the following parameters:

- Frame rate of ADNS-3080 sensor: 6469 fps
- Shutter speed of ADNS-3080 sensor: self-adjust (i.e., automatic)
- Resolution of ADNS-3080 sensor: 400 cpi
- Camera lens on ADNS-3080 sensor: 17 mm (M12, F4.2)
- Data output rate from mbed microcontroller: 100 Hz

- Distance from ADNS-3080 sensor to moving roadway: 9” (229 mm)

2.6 Constant Speed, Constant Angle Tests

The purpose of the tests was to understand the relationship between the outputs of the ADNS-3080 mouse sensor and the speed of the moving roadway. The tests were designed to test if ADNS-3080 sensors can output consistent motion data over a wide range of speeds and at different slip angles. A wide range of speeds were conducted in the tests (Table 2.1). For every moving roadway speed, the servo motor moved from -45° to 45° with an increment of 3°, and it stayed for 2 minutes to allow data collection at each encoder angle position.

Table 2.1 Speeds conducted in constant speed, constant angle tests.

Test bed DC motor speed	Actual moving roadway speed
200 rpm	2.75 MPH (1.23 m/sec)
350 rpm	4.81 MPH (2.15 m/sec)
500 rpm	6.89 MPH (3.08 m/sec)
750 rpm	10.31MPH (4.61 m/sec)
1000 rpm	13.76 MPH (6.15 m/sec)
1250 rpm	17.20 MPH (7.69 m/sec)
1500 rpm	20.65 MPH (9.23 m/sec)
1750 rpm	24.09 MPH (10.77 m/sec)
2000 rpm	27.51 MPH (12.30 m/sec)
2500 rpm	34.40 MPH (15.38 m/sec)
3000 rpm	41.29 MPH (18.46 m/sec)
3500 rpm	48.16 MPH (21.53 m/sec)

The output of the ADNS-3080 mouse sensor (Δx and Δy) was used to calculate speed of the moving roadway. Δx, Δy is motion at each time interval of 10 msec. Since the mouse sensor had twice the data output rate than the encoder, mouse sensor speed measurements were averaged between encoder measurements (Figure 2.7). This would ensure that both data sets had the same number of data points. The data was then curve-fit using a linear regression model against the actual speed of the moving roadway (measured by the encoder).

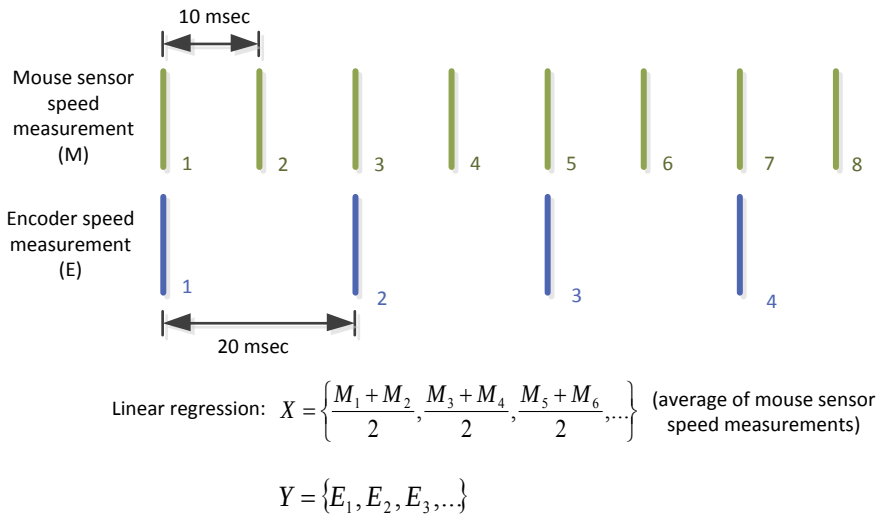

Figure 2.7 Averaging of mouse sensor data for linear regression analysis.

The linear regression model was performed forcing the y intercept to be zero. Thus, the relationship can be expressed using the following equation:

$$S_{road} = \beta \times S_{mouse}$$

where S_{road} is the speed of the moving roadway, S_{mouse} is the speed measurements of the ADNS-3080 sensor (in dimensionless counts of Δx and Δy). Please note that S_{road} can either be in MPH or m/sec and the value of the speed constant β would change accordingly.

The results are shown in Figure 2.8 and Appendix A. For the entire ranges of slip angles and moving roadway speeds (measured in m/sec), the ADNS-3080 sensor had an overall mean speed constant (β) of 0.069214 with a standard deviation of 0.000629 (or 0.91% of the mean).

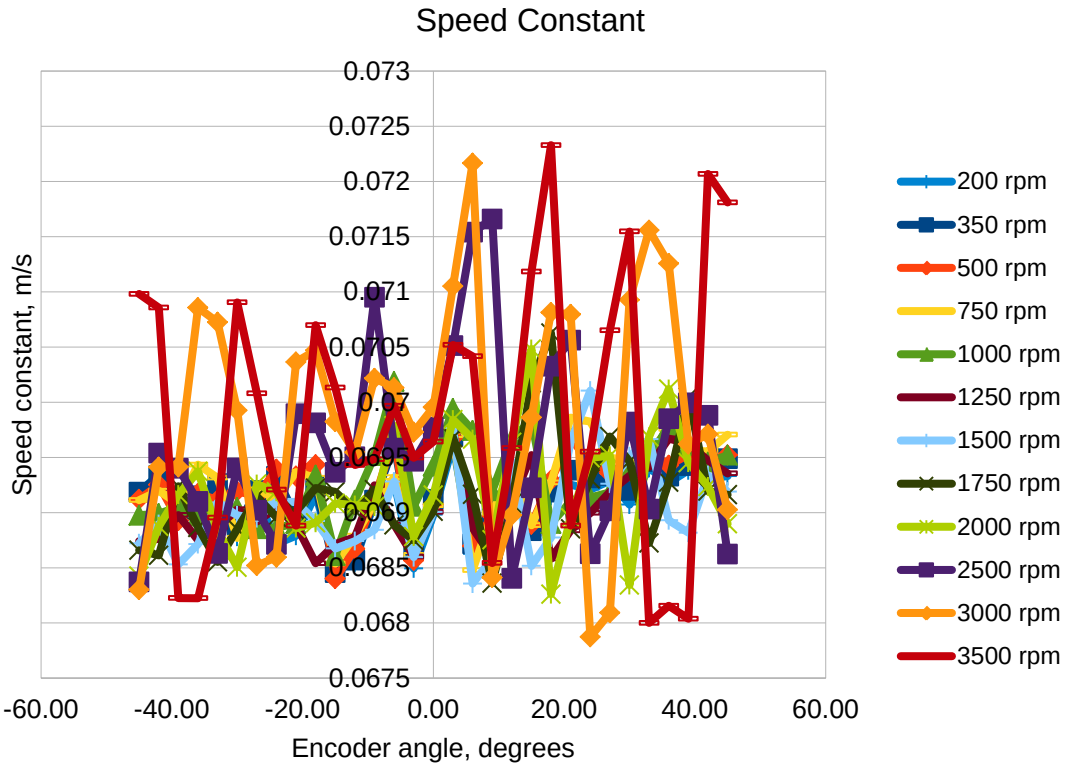

Figure 2.8 Calculated speed constants of ADNS-3080 sensor, representation for two of four operational quadrants.

The output of the mouse sensor (Δx and Δy) was also used to calculate angular measurements. The results were used to compare against the slip angles generated by the servo motor. The data was averaged over the 2 minute data collection period for each moving roadway speed and each slip angle position. The results are shown in Figure 2.9 and Appendix B.

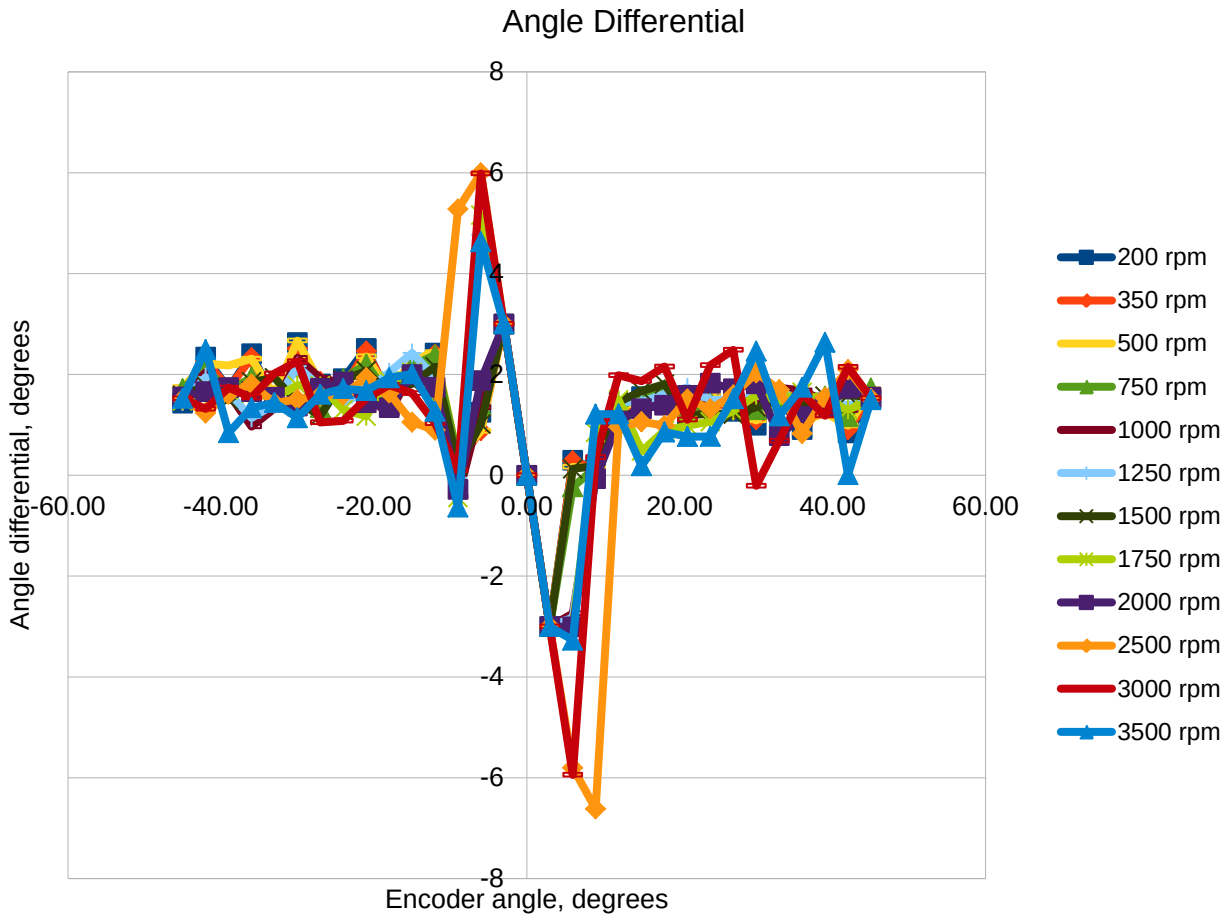

Figure 2.9 Calculated angle measurements of ADNS-3080 sensor.

It was noticed that there is a deadband in the data between -10° and 10°. This feature is by design from the manufacturer of the mouse sensor to prevent the mouse from "wandering" near the center position when there is little or no movement. Outside of the deadband, the mouse sensor had an overall mean angular measurement error of 1.245° with a standard deviation of 1.418°.

Sensor Behavior in Deadband

Additional tests were conducted to study the behavior of ANDS-3080 sensor in the deadband. In the tests, the servo motor moved from -10° to 10° with an increment of 1°, and it stayed for 2 minutes to allow data collection at each encoder angle position. Three different moving roadway speeds were tested: 750 rpm (10.31 MPH or 4.61 m/sec), 1500 rpm (20.65 MPH or 9.23 m/sec), and 2500 rpm (34.40 MPH or 15.38 m/sec). Figure 2.10 shows the results.

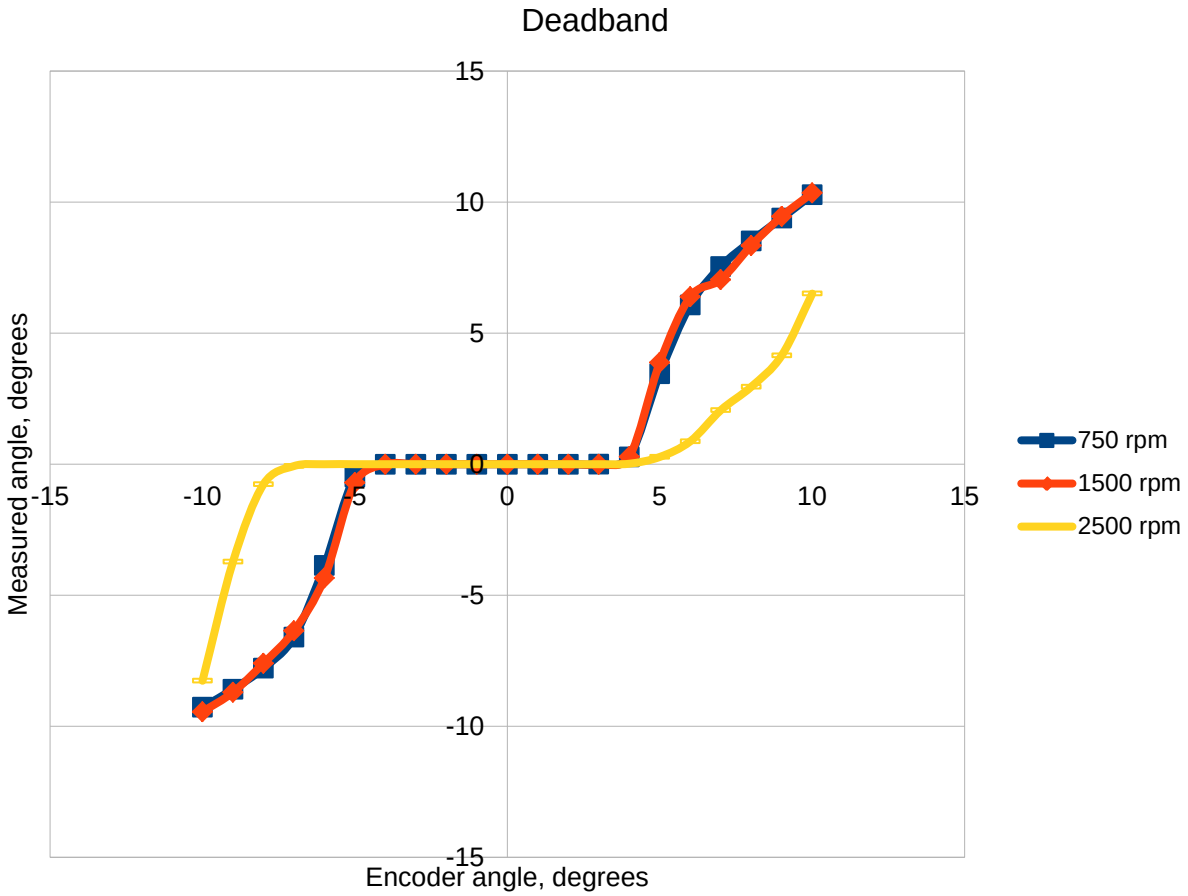

Figure 2.10 ADNS-3080 sensor behavior in the deadband.

It was observed that the sensor had low (or no) sensitivity between -5° and 5° at lower speeds (750 rpm and 1500 rpm). As the speed increased to 2500 rpm, the insensitivity region grew to −10° and 10°. To avoid deadbands, the mouse sensor should be physically rotated before mounting on a vehicle to be used as a velocity sensor.

2.7 Linear Speed Tests

The purpose of the tests was to understand the relationship between the measurements of the mouse sensor and the actual speeds of the moving roadway. In the tests, the servo motor was fixed at a specific slip angle while the speed of the moving roadway was decreased from 4000 down to 0 rpm (55.05 ~ 0 MPH or 24.61 ~ 0 m/sec). The duration of each test run was 900 seconds at a deceleration rate of 0.09 ft/sec^2 (0.027 m/sec^2).The tests were designed to find out if there is a linear relationship between the output of the mouse sensor (Δx and Δy) and the actual speeds of the moving roadway. The measurements of the mouse sensor were recorded and the tests were repeated for the servo motor to change the slip angle from -45° to 45° with an increment of 9°. A linear regression analysis, which forcing the y intercept to be zero, was then performed on each data set and the relationship can be expressed using:

$$S_{road} = \beta \times S_{mouse}$$

where S_{road} is the speed of the moving roadway in MPH or m/sec, S_{mouse} is the speed measurement of the ADNS-3080 sensor (in dimensionless counts of Δx and Δy). Please note that the value of speed constant β would change based on the unit of S_{road}.

The results of the linear regression analysis are shown in Table 2.2 and Appendix C. Please note that since measurements made within the deadband were neither reliable nor accurate, they were excluded from the results.

Table 2.2 Results of the speed analysis of ADNS-3080 sensor.

Encoder angle	β (in m/sec)	R^2
-45°	0.073249	0.999667
-36°	0.0736103	0.999367
-27°	0.073221	0.999657
-18°	0.073444	0.999626
18°	0.074054	0.998737
27°	0.073129	0.999619
36°	0.073362	0.999485
45°	0.073481	0.999363

2.8 Swept Angle Accuracy Tests

The purpose of these tests was to understand how accurately can the mouse sensor measure angles. The servo motor was programmed to sweep through a range of angles and measurements made by the mouse sensor were compared with encoder readings on the servo motor. Several different rounds of tests were performed to measure the angle accuracy of the mouse sensor under different scenarios:

1. The mouse sensor was tested for a full 360° sweep with a 3° increment (i.e., 120 discrete angle positions).
2. Tests with a 1° increment with 20° range sweep were conducted.
3. Tests were performed with different configurations to see if any or combinations of different configuration parameters would affect the performance of the mouse sensor:
    a. Different mouse chip data rates (100 Hz, 20 Hz),
    b. Different sensor resolutions (400 cpi, 1600 cpi),
    c. Different distances from the mouse sensor to the moving roadway (9” or 229 mm, 6” or 152 mm, and 4” or 102 mm),
    d. Lenses with different focal lengths (17 mm (F4.2), 25 mm (F2.5)).

Details and results of each test are described in the following sections.

Round 1

In this test, the servo motor moved from -180° to 180° with an increment of 3°, and it stayed for 1 minute to allow data collection at each encoder angle position. Three different moving roadway speeds were tested: 750 rpm (10.31 MPH or 4.61 m/sec), 1500 rpm (20.65 MPH or 9.23 m/sec), and 2500 rpm (34.40 MPH or 15.38 m/sec). In this test, the mouse sensor had a data output rate of 100 Hz. The sensor was located at 9" (229 mm) above the moving roadway with a 17 mm lens and the resolution was set at 400 cpi.

Please note that data within deadbands (every 90°) was removed from the table and the figure. At 750 rpm, the mouse sensor had a mean sensor error of 1.396° with a standard deviation of 0.030°. At 1500 rpm, the mouse sensor had a mean sensor error of 1.390° with a standard deviation of 0.018° and at 2500 rpm, the sensor error was 1.442° with a standard deviation of 0.024°. Table 2.3 summarizes the results, Figure 2.11 shows the plot, and Appendix D show the detailed results for each encoder angle tested.

Table 2.3 Summary of angle measurements at different moving roadway speeds (750 rpm, 1500 rpm, 2500 rpm).

Moving Roadway Speed	Mean Sensor Error	Standard deviation
750 rpm	1.396°	0.030°
1500 rpm	1.390°	0.018°
2500 rpm	1.442°	0.024°

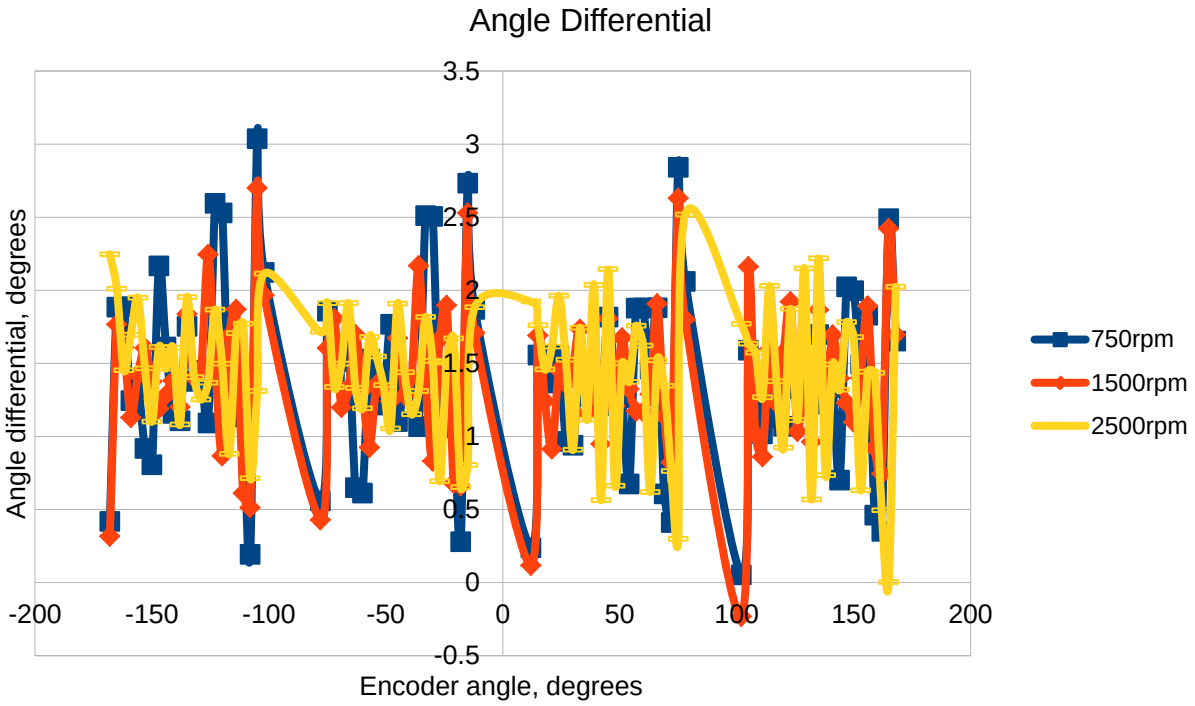

Figure 2.11 Results of angle measurements at different moving roadway speeds (750 rpm, 1500 rpm, 2500 rpm).

Round 2

In this test, the servo motor moved from -130° to -110° with an increment of 1°, and it stayed for 1 minute to allow data collection at each encoder angle position. Three different moving roadway speeds were tested: 750 rpm (10.31 MPH or 4.61 m/sec), 1500 rpm (20.65 MPH or 9.23 m/sec), and 2500 rpm (34.40 MPH or 15.38 m/sec). The mouse chip microcontroller was also reconfigured to allow either 100Hz or 20Hz data rate output to compare the results. Other settings remained unchanged: the sensor was located at 9" (229 mm) above the moving roadway with a 17 mm lens and the resolution was set at 400 cpi.

At 100 Hz data output rate, the mouse sensor had a measurement error of 1.536° (with a standard deviation of 0.304°), and at 20 Hz data rate, the error was 1.499° (with a standard deviation of 0.090°). Table 2.4 summarizes the results and detailed results are shown in Appendix E.

Table 2.4 Summary of angle measurements at different data rates.

Data Rate	Mean Sensor Error	Standard deviation
100 Hz	1.536°	0.304°
200 Hz	1.499°	0.090°

Round 3

In this test, the mouse sensor was lowered to 4" (102 mm) above the moving roadway to enable the sensor to pick up more surface texture details. The data rate was changed back to 100 Hz as there was no significant gain in (mean) angle measurements between 100 Hz and 20 Hz data output rate. Other settings remained unchanged: the sensor was equipped with a 17 mm lens and the resolution was set at 400 cpi.

At 750 rpm, the mean sensor error was 1.421° (with a standard deviation of 0.273°). At 1500 rpm, the error was 1.478° (with a standard deviation of 0.332°), and at 2500 rpm, the error was 2.019° (with a standard deviation of 0.208°). Table 2.5 summarizes the results and detailed results are shown in Appendix F.

Table 2.5 Summary of angle measurements at 4" (102 mm) above the moving roadway

Moving Roadway Speed	Mean Sensor Error	Standard deviation
750 rpm	1.421°	0.273°
1500 rpm	1.478°	0.332°
2500 rpm	2.019°	0.208°

Round 4

In this test, the resolution of the mouse sensor was increased from 400 to 1600 cpi. The distance between the sensor and the moving roadway remained at 4" (102 mm). Other settings remained unchanged: the sensor was equipped with a 17 mm lens and the data rate was set at 100 Hz.

At 1600 cpi, the mean sensor error was 1.219° (with a standard deviation of 0.157°), 0.938° (with a standard deviation of 0.139°), and 0.969° (with a standard deviation of 0.109°) for the speeds of 750 rpm, 1500 rpm, and 2500 rpm, respectively. Table 2.6 summarizes the results and detailed results are shown in Appendix G.

Table 2.6 Summary of angle measurements at 1600 cpi and 4" (102 mm) above moving roadway.

Moving Roadway Speed	Mean Sensor Error	Standard deviation
750 rpm	1.219°	0.157°
1500 rpm	0.938°	0.139°
2500 rpm	0.969°	0.109°

Round 5

The performance of the mouse sensor was improved when the resolution was changed to 1600 cpi. However, since 4" (102 mm) was too close to the roadway and not practical to be implemented on a vehicle. Therefore, in this test, the height of the mouse sensor was raised back to 9" (229 mm) and the sensor resolution remained at 1600 cpi. Other settings stayed unchanged: the sensor was equipped with a 17 mm lens and the data rate was set at 100 Hz.

At 750 rpm, the mean sensor error was 1.885° (with a standard deviation of 0.366°). At 1500 rpm, the error was 1.445° (with a standard deviation of 0.202°) and the error was 1.396° (with a standard deviation of 0.140°) at 2500 rpm. Table 2.7 summarizes the results and detailed results are shown in Appendix H.

Table 2.7 Summary of angle measurements at 1600 cpi and 9" (229 mm) above moving roadway.

Moving Roadway Speed	Mean Sensor Error	Standard deviation
750 rpm	1.885°	0.366°
1500 rpm	1.445°	0.202°
2500 rpm	1.396°	0.140°

Figures 2.12 ~ 2.14 show aggregated plots of results for tests conducted from Round 2 to Round 5.

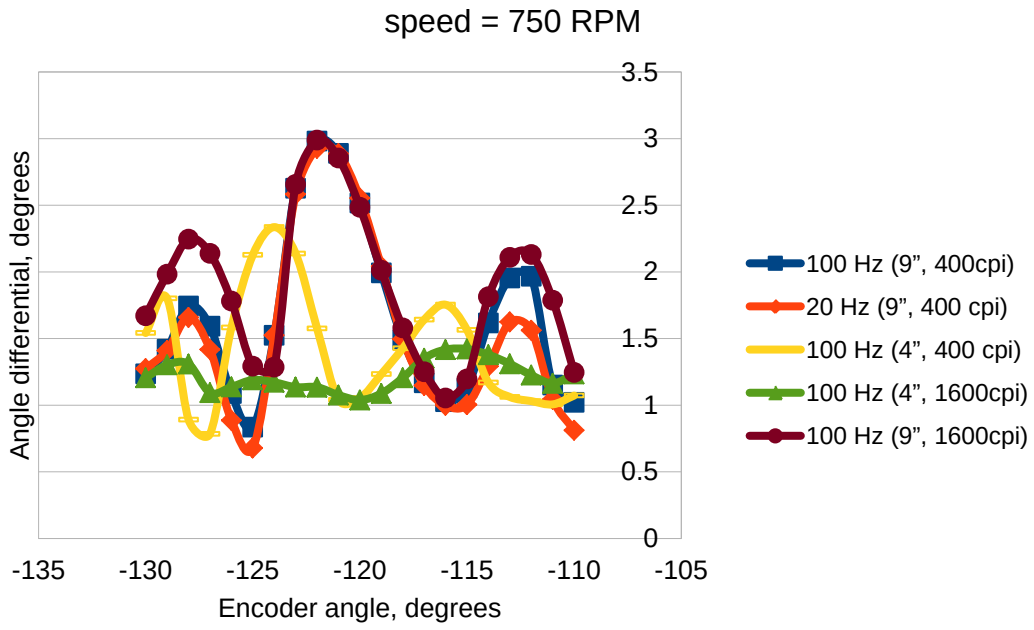

Figure 2.12 Results of angle measurements at speed = 750 rpm with different mouse sensor resolutions (400cpi, or 1600cpi) and sensor distances (4" or 9").

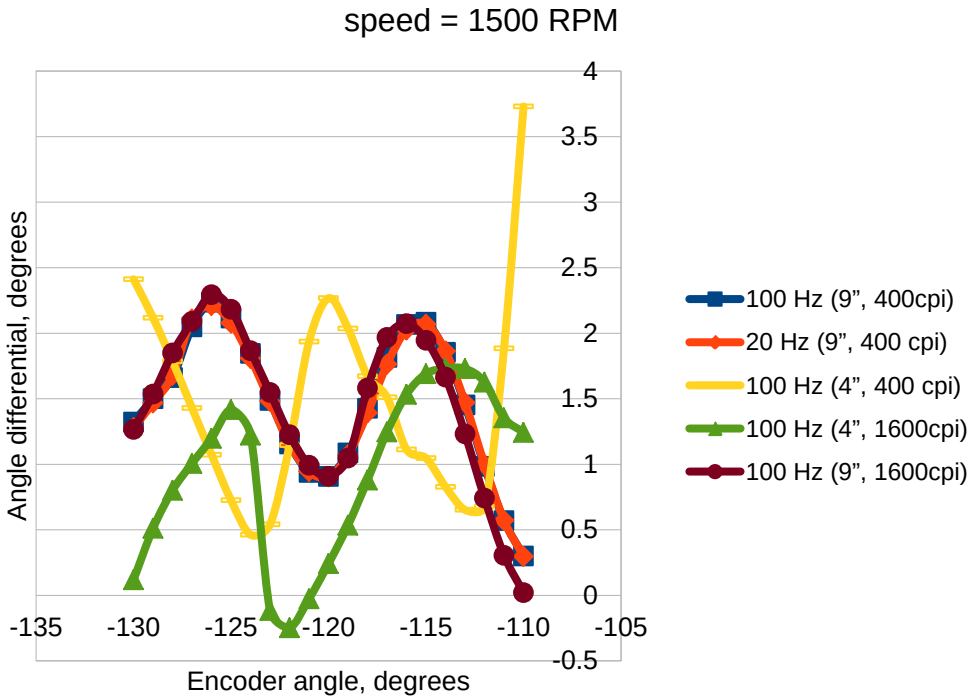

Figure 2.13 Results of angle measurements at speed = 1500 rpm with different mouse sensor resolutions (400cpi, or 1600cpi) and sensor distances (4” or 9”).

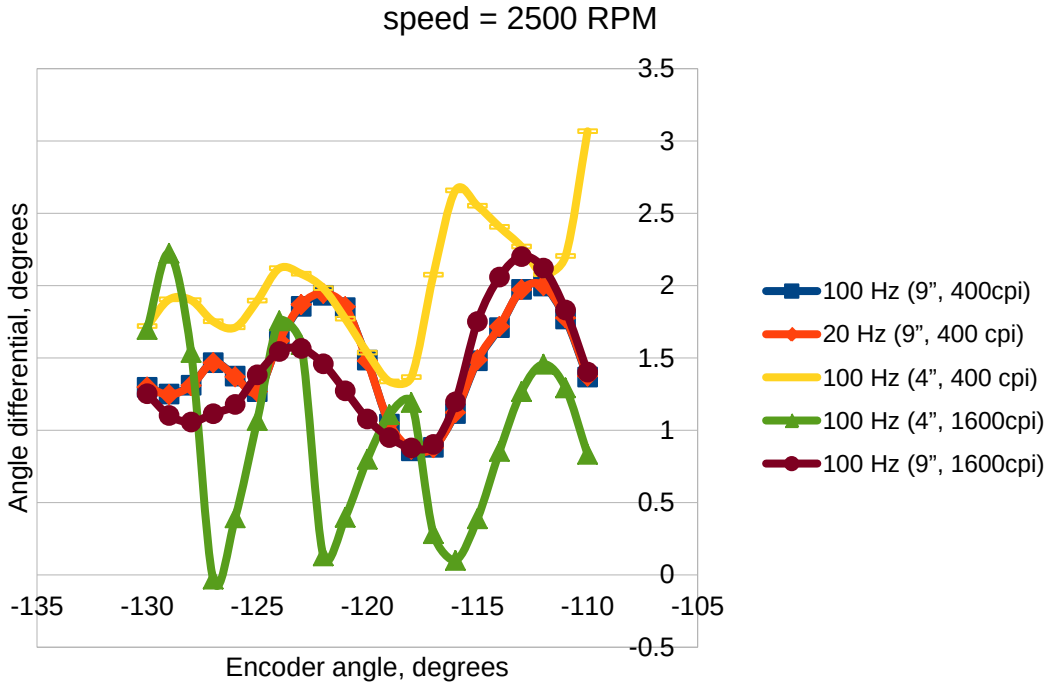

Figure 2.14 Results of angle measurements at speed = 2500 rpm with different mouse sensor resolutions (400cpi, or 1600cpi) and sensors distances (4” or 9”).

Round 6

In this test, the 17 mm (F4.2) lens on the mouse sensor was replaced with a 25 mm (F2.5) lens. Other settings remained unchanged: the sensor was located at 9" (229 mm) above the moving roadway and the data rate was set at 100 Hz with a resolution of 1600cpi.

With a lens with longer focal length (i.e., more zoom power), the mean sensor error was 2.063° (with a standard deviation of 0.414°), 1.439° (with a standard deviation of 0.345°), and 1.501° (with a standard deviation of 0.322°) for the speeds of 750 rpm, 1500 rpm, and 2500 rpm, respectively. Table 2.8 summarizes the results and detailed results are shown in Appendix I. Figure 2.15 shows the plot.

Table 2.8 Summary of angle measurements with 25 mm lens and 9" (229 mm) above moving roadway.

Moving Roadway Speed	Mean Sensor Error	Standard deviation
750 rpm	2.063°	0.414°
1500 rpm	1.439°	0.345°
2500 rpm	1.501°	0.322°

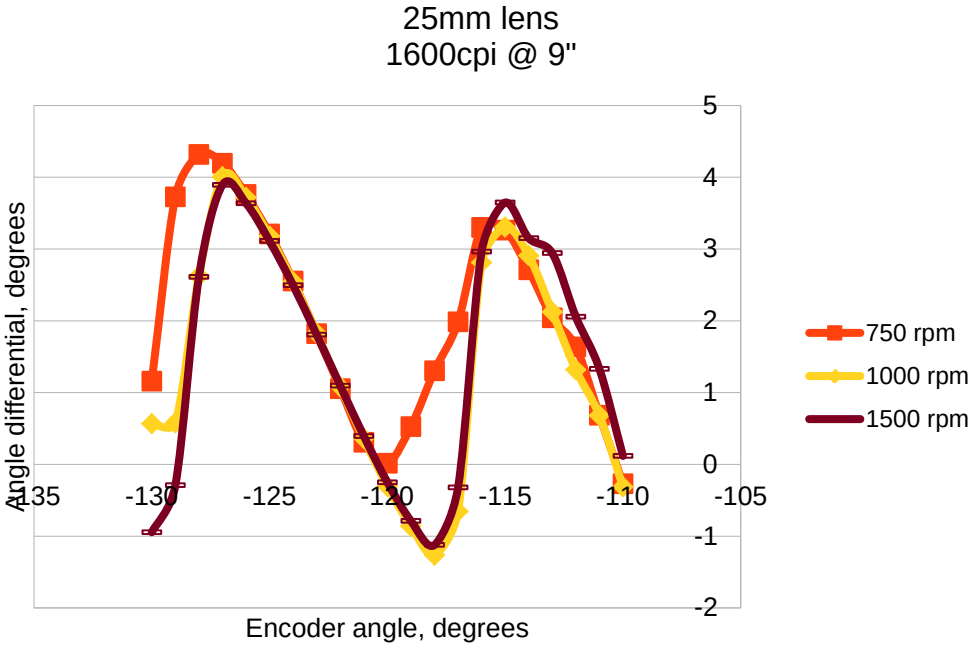

Figure 2.15 Results of angle measurements with 25 mm lens at a 9" distance to the moving roadway.

Round 7

In this test, the lens was changed back to 17 mm and the height of the mouse sensor was lower down to 4" (102 mm). Additional moving roadway speeds were tested to see if the mouse sensor performed better at lower speeds (less than 1500 rpm). Other settings remained unchanged: the sensor had a resolution of 1600 cpi and the data output rate was set at 100 Hz.

Table 2.9 summarizes the results and detailed results are shown in Appendix J. Figure 2.16 shows the angle differential plot.

Table 2.9 Summary of angle measurements with 17 mm lens and 4" (102 mm) above moving roadway.

Moving Roadway Speed	Mean Sensor Error	Standard deviation
350 rpm	1.326°	0.271°
750 rpm	1.144°	0.160°
10000 rpm	1.246°	0.123°
1200 rpm	1.971°	0.269°
1500 rpm	0.906°	0.159°

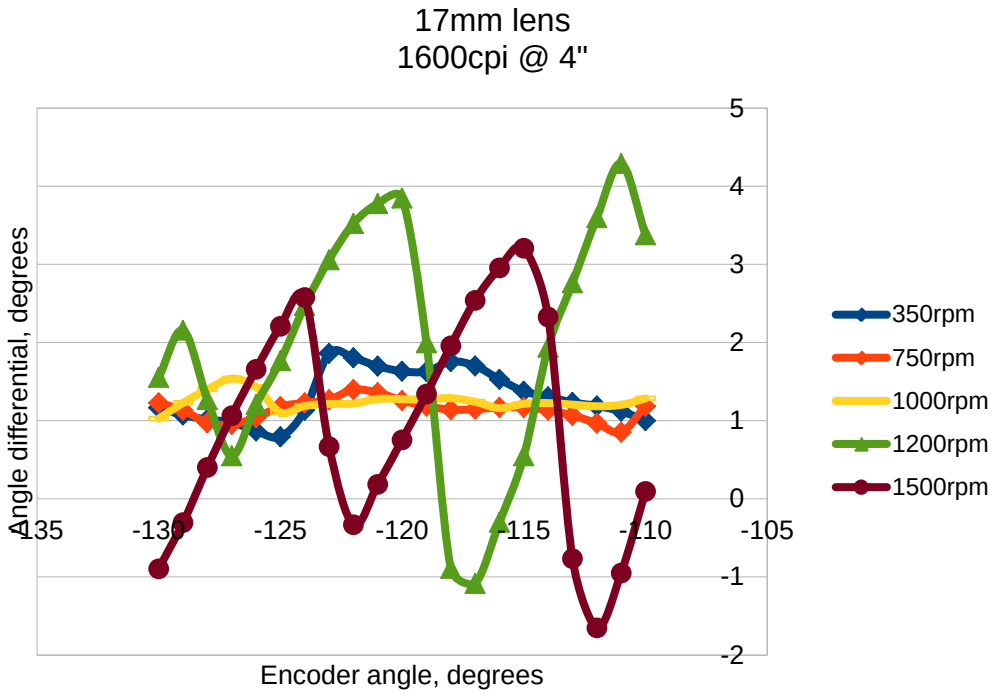

Figure 2.16 Results of angle measurements with 17 mm lens at a distance 4" to the moving roadway.

Round 8

In this test, the lens was changed to 25 mm and the height of the mouse sensor was raised to 6" (152 mm). This was to test the hypothesis that the mouse sensor should have similar performance with 17 mm lens at 4" (102 mm) above the moving roadway and 25 mm lens at 6" (152 mm) above the moving roadway because the coverage area of the camera for both configurations are about the same. Other settings stayed unchanged: the sensor had a resolution of 1600 cpi and the data output rate was set at 100 Hz.

Table 2.10 summarizes the results and detailed results are shown in Appendix K. Figure 2.17 shows the angle differential plot.

Table 2.10 Summary of angle measurements with 25 mm lens and 6" (152 mm) above moving roadway.

Moving Roadway Speed	Mean Sensor Error	Standard deviation
350 rpm	1.720°	0.428°
750 rpm	1.439°	0.200°
10000 rpm	1.566°	0.435°
1500 rpm	0.837°	0.136°

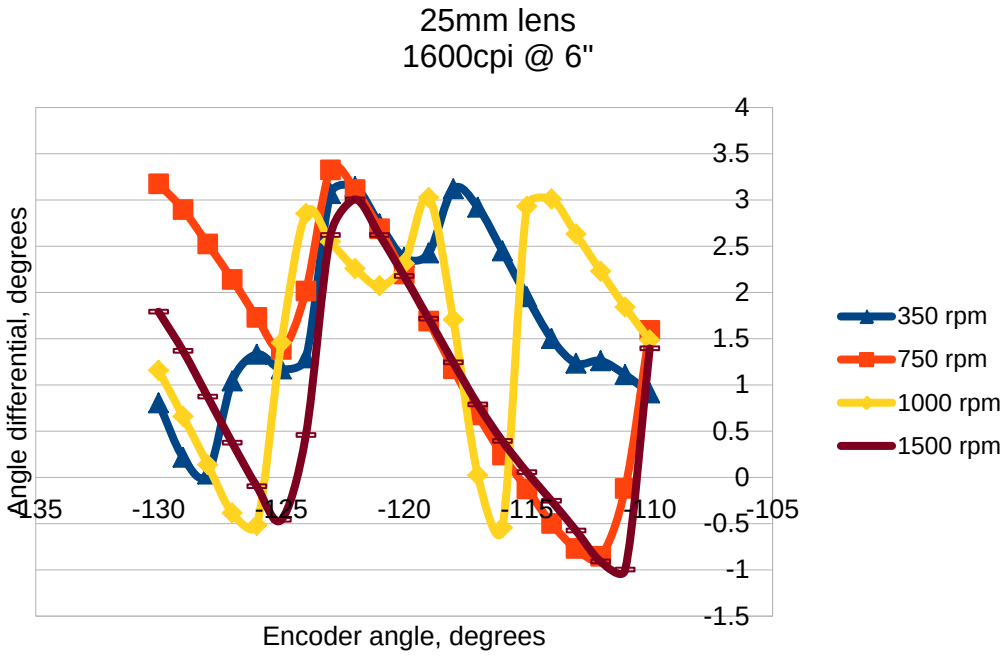

Figure 2.17 Results of angle measurements with 25 mm lens at a distance 6" to the moving roadway.

2.9 Discussion

In Section 2.6, the ADNS-3080 mouse sensor was evaluated over a wide range of moving roadway speeds from 200 rpm (2.75 MPH or 1.23 m/sec) to 3500 rpm (48.25 MPH or 21.57 m/sec) and over a wide range of yaw angles from -45° to 45°. In the speed analysis, it was found that the mouse sensor has a mean speed constant (β) of 0.069214 with a standard deviation of 0.000629 (or 0.91%) if measured in m/sec. In the angle analysis, it was found that the mouse sensor has a deadband between -10° and 10°. It was later observed that the deadband exists in every quadrant. This feature is by design to prevent the mouse from drifting to the left or right when the mouse is moved up or down, or vice versa. However, this feature is not desired when the mouse sensor is planned to be used as a velocity sensor on a vehicle. To avoid the deadband, the sensor can be physically rotated. Since a speed sensor on a vehicle does not need to have the full 90° range of measurement, the mouse sensor was rotated 45° and thus creating a velocity sensor with an effective range of 70° (Figure 2.18). Excluding the deadband observed in the testing, the mouse sensor was found to have a mean sensor error of 1.245° with a standard deviation of 1.418° (at 400 cpi).

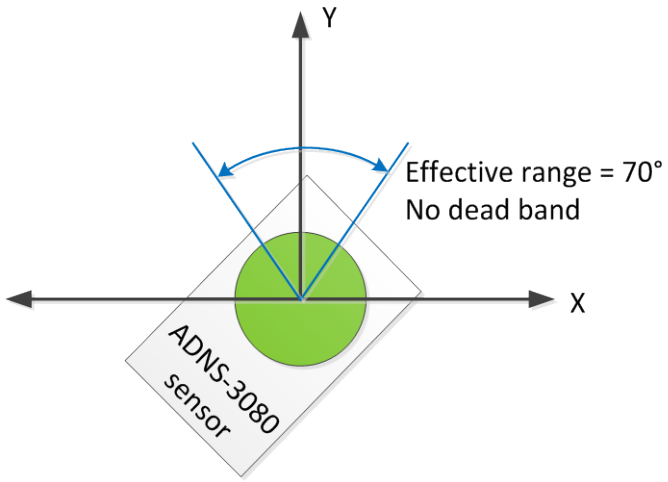

Figure 2.18 Rotation of mouse sensor to avoid the deadband.

In Section 2.7, a different test was performed to find the relationship between the measurements made by the ADNS-3080 mouse sensor and the actual speeds of the moving roadway. After the linear regression analysis, it was found that the values of the coefficient of determination (R^2) were all greater than 0.999 under all conditions tested. This indicates that the measurements of ADNS-3080 mouse sensor are linearly proportional to the actual speeds of moving roadway. The results found that the mouse sensor has a speed constant (β) from 0.073221 to 0.074054, which is similar to the findings in Section 2.6.

From Section 2.6, it was found that the angle measurements of ADNS-3080 mouse sensor can be off as much as 5° in the worst case scenario. In Section 2.8, different parameters of the sensor were changed to find out if the performance of angle measurement can be improved:

- Data showed that there was no significant performance change if the data output rate of the mouse sensor was changed from 100 Hz to 20 Hz (mean sensor error of 1.536° vs. 1.499°).
- Data showed that there was no performance improvement when the mouse sensor was moved closer to the moving roadway in order for the camera to detect more surface texture details. The distance between the mouse sensor and the moving roadway was moved from 9" (229 mm) to 4" (102 mm), and the field of view was decreased from 0.75" × 0.75" (19 × 19 mm) to 0.39" × 0.39" (9.9×9.9 mm) (with the same camera resolution), however, the result was no better than what was found in Section 2.6 and the mean sensor error at 4" (102 mm) was 1.639°.
- Data showed that the performance of the mouse sensor improved when the resolution of the sensor was increased from 400 to 1600 cpi. At 4" (102 mm) above the moving roadway, the mean sensor error was improved from 1.639° to 1.042°. More importantly, the standard deviation was decreased from 0.271° to 0.135°. This means that the mouse sensor is performing at a higher consistency (because of a lower standard deviation), thus producing more reliable results.
- Data showed that the error of the mouse sensor decreased when the sensor was moved back to 9" above the moving roadway. At 9" above the moving roadway, the mean sensor error was at 1.575° and the standard deviation was 0.236°. This result still compared favorably than the results when the resolution of the mouse sensor was set at 400 cpi because the standard deviation was decreased from 1.034° to 0.236°.
- Data showed that there was no performance improvement when the 17 mm lens was replaced with a 25 mm lens. With a 25 mm lens, the mouse sensor covered a smaller area of 0.51" × 0.51" (12.9 × 12.9 mm), and can detect more surface details than a 17 mm lens. However, this change was not beneficial to the performance of the mouse sensor.
- Additional tests with 17 mm lens at 4" above the roadway and 25 mm lens at 6" (152 mm) above the roadway did not show much improvement in mouse sensor performance. The mean sensor error was 1.319° with 17 mm lens at 4" (102 mm) above the roadway, and 1.391° with 25 mm lens at 6" (152 mm) above the roadway.

Please note that the small differences in all mean sensor measurement errors could be partially due to sensor mounting bias. Best efforts were made to make sure that the sensor was mounted in parallel to the moving roadway. However, a small mounting bias could translate into differences in mean sensor measurement errors. The standard deviation of sensor measurements should also be used as a performance indicator. A small standard deviation number shows that the sensor is tracking reliably and consistently.

In summary, the ADNS-3080 mouse sensor seems had better and more consistent performance when the resolution was set at 1600 cpi. The performance did not change much with a longer focal length lens (i.e., higher zoom power). The performance did improve slightly when the mouse sensor was moved closer to the moving roadway. However, to prevent the mouse sensor and the light source from hitting or scraping the ground on a moving vehicle, it was found that the mouse sensor should not be mounted lower than 9" (228 mm) above the ground on a vehicle.

Chapter 3. Field Evaluation of ADNS-3080 Sensor

3.1 Equipment Setup

A 4”×2”×4.25” (100 mm×50 mm×107 mm) weather-proof aluminum box was constructed to house the ADNS-3080 mouse sensor and the mbed microcontroller. Figure 3.1 shows the box.

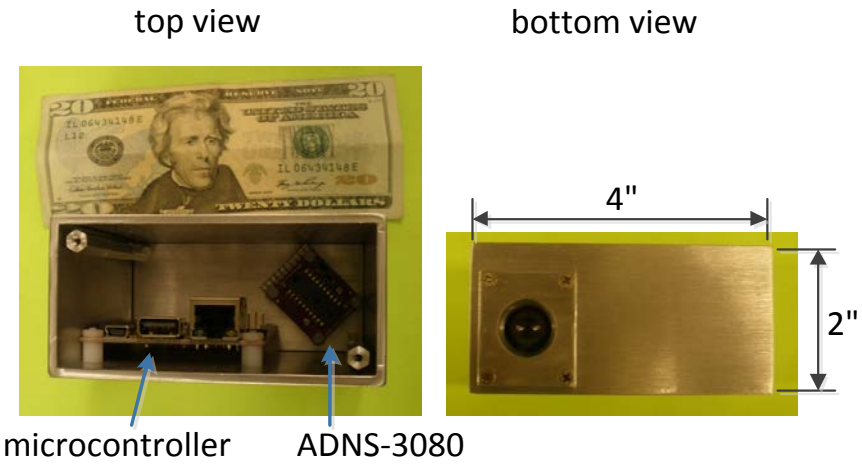

Figure 3.1 ADNS-3080 sensor box for field tests.

The sensor box was mounted at the front grille of a vehicle beneath the license plate. The distance between the ADNS-3080 mouse sensor and the ground was 9” (229 mm) (to match the setup with the in-lab testing). A housing with a Philips halogen light bulb (same one that was used in the testbed) was attached to the sensor box and hanging in front of the sensor box to provide illumination. Figure 3.2 shows the setup.

Figure 3.2 Field testing equipment setup.

3.2 Experimental Design

Similar to the in-lab testing, field testing was designed to evaluate the performance of ADNS-3080 mouse sensor on different types of road surfaces, including paved asphalt roads and unpaved dirt roads. Tests were conducted with the following parameters:

- Frame rate of ADNS-3080 sensor: 6469 fps
- Shutter speed of ADNS-3080 sensor: self-adjust (i.e., automatic)
- Resolution of ADNS-3080 sensor: 1600 cpi
- Camera lens on ADNS-3080 sensor: 17 mm (M12, F4.2)
- Data output rate from mbed microcontroller: 100 Hz
- Distance from ADNS-3080 sensor to moving roadway: 9” (229 mm)

In the field evaluation, a NovAtel SPAN system was used as a reference for vehicle positions and velocities. The SPAN system includes a dual-frequency GPS receiver and a Honeywell HG1700-AG58 IMU. By integrating GPS and IMU together, the system can provide accurate position and velocity data even when a vehicle passes under a bridge and GPS signals are not available for a short period of time. When the SPAN system has a clear view of the sky, it can utilize GPS correctional signals from IVLAB’s Virtual Reference Station (VRS) network and maintain a positional accuracy of 1” (2.5 cm) or better. If GPS signals are lost, it was found from previous testing that the SPAN system can maintain a positional accuracy of less than 4” (10 cm) after 20 seconds of GPS outage [15]. Figure 3.3 shows a NovAtel SPAN system mounted on top of a vehicle.

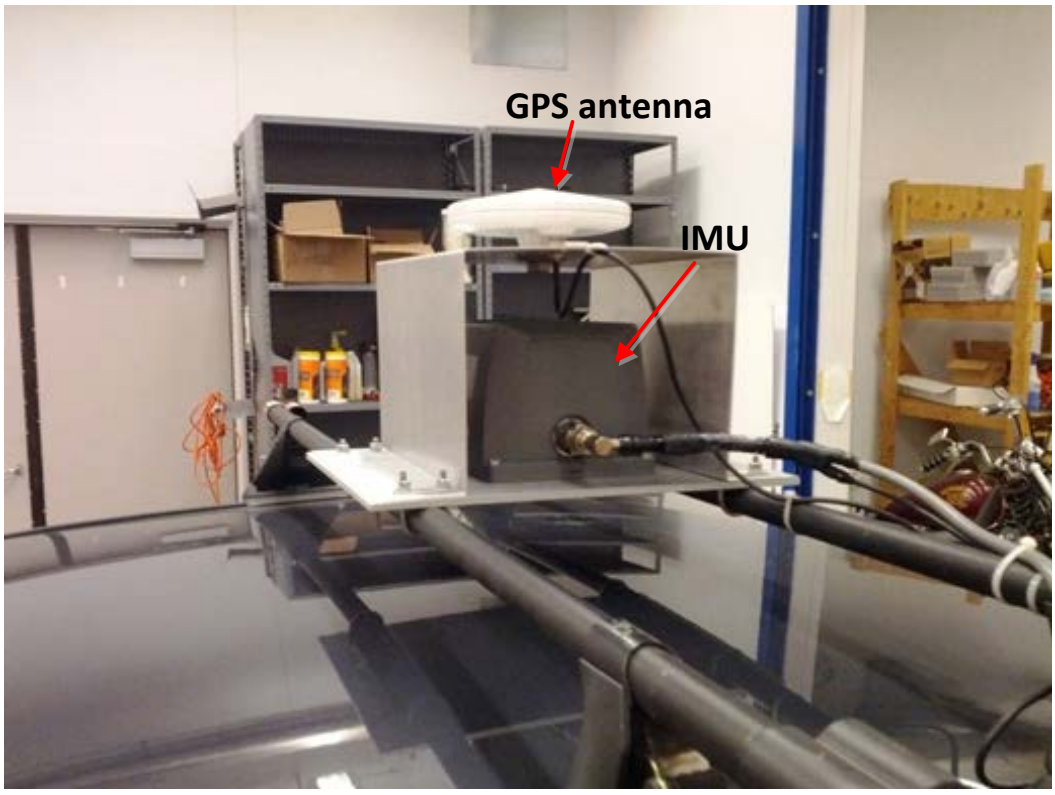

Figure 3.3 NovAtel SPAN system mounted on top of a vehicle.

3.3 Field Evaluation on Paved Asphalt Roads

The field evaluation on paved asphalt roads was conducted between Kasota Avenue and Energy Park Drive between Minneapolis and St. Paul in Minnesota. The route was about 4.1 miles (6.6 km) long and it is shown in Figure 3.3. The weather was sunny and to partly cloudy and the road condition was dry.

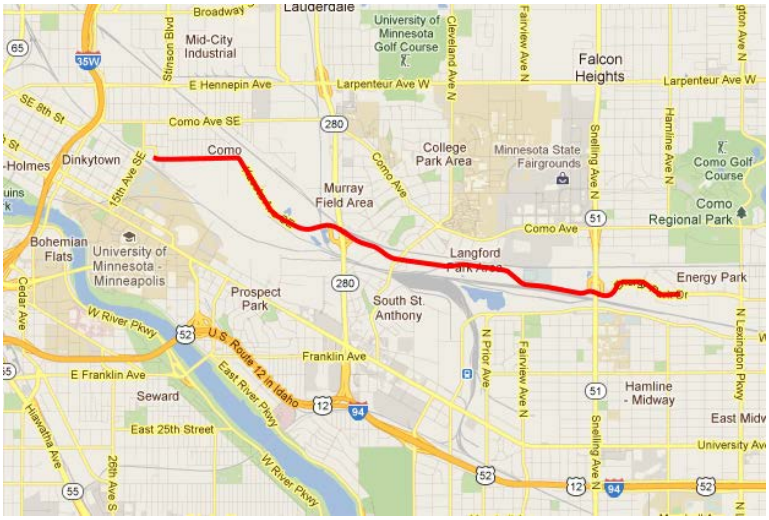

Figure 3.4 Route of field evaluation on paved asphalt roads (Source: Google Maps, ©2012 Google, Sanborn).

Data Analysis

By using the method described in Section 2.7, a linear regression analysis, which forcing the y intercept to be zero, was performed to find the relationship between speed measurements of the ADNS-3080 mouse sensor and the SPAN system. The SPAN system had a data output rate of 10 Hz, which was only one third the data rate of the mouse sensor. Therefore, the mouse sensor data was averaged between outputs of each SPAN data point (i.e., the same method as described in Figure 2.7) before linear regression analysis was applied.

The result of the linear regression analysis can be expressed using the following equation:

$$S_{SPAN} = \beta \times S_{mouse}$$

where S_{SPAN} is the speed output of the SPAN system in MPH or m/sec, S_{mouse} is the speed measurements of the ADNS-3080 sensor (in dimensionless counts of Δx and Δy). Please note that the constant β would have different values for different speed units.

Two data runs were performed and the results of the linear regression analysis are shown in Table 3.1 and Figure 3.5. Please note that the β constant found in the field evaluation was different from the β constant found in Section 2.7. This was mainly due to the resolution change from 400 cpi to 1600 cpi in the mouse sensor and the camera lens was re-adjusted in order to focus on the road surface better.

Table 3.1 Results of the speed analysis of ADNS-3080 sensor on paved roads.

Data run	β (in m/sec)	R-Square
1	0.035619	0.983492
2	0.035499	0.981289

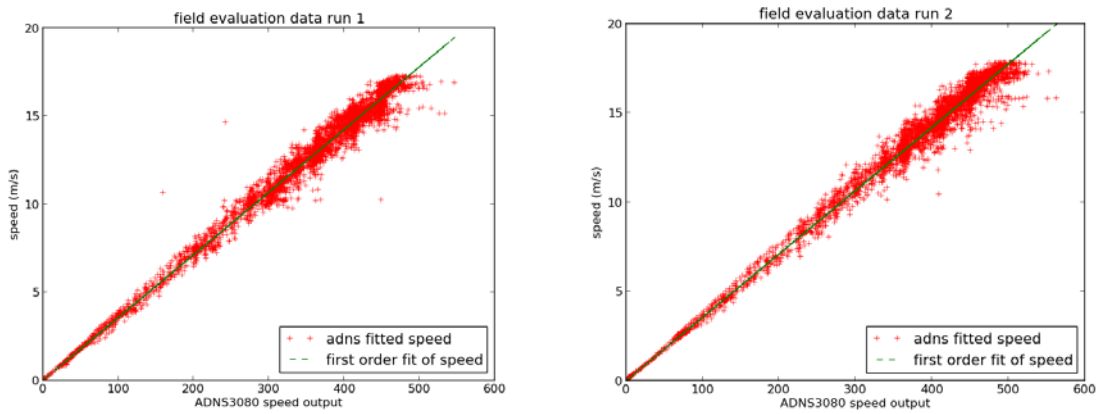

Figure 3.5 Results of field evaluation of ADNS-3080 and fitted speed data on paved roads.

Angle measurements of ADNS-3080 mouse sensor were also analyzed to compare against heading angles computed from the SPAN data. Since the ADNS-3080 sensor was rotated 45° inside the field sensor box, a rotation matrix was applied so that the calculated angle measurements of ADNS-3080 matched with the local vehicle coordinate system (and the SPAN coordinate system). Results of angle analysis of the two data runs are shown in Table 3.2 and Figure 3.6. Please note that the computed angles from the SPAN system were used as reference and the angle differential $\Delta\theta_i$ is calculated as:

$$\Delta\theta_i = ADNS3080\theta_i - SPAN\theta_i$$

Table 3.2 Results of the angle analysis of ADNS-3080 sensor on paved roads.

Data run	Δθ (mean)	Δθ (standard deviation)
1	-1.859409°	1.374962°
2	-1.633810°	1.211004°

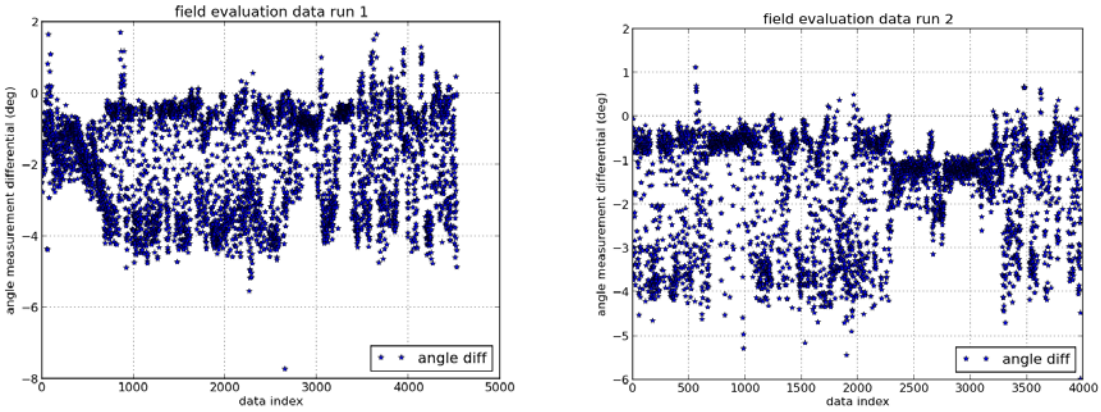

Figure 3.6 Results of field evaluation of ADNS-3080 and angle measurement (differential) data on paved roads.

3.4 Field Evaluation on Dirt Roads

Field evaluation of ADNS-3080 mouse sensor was also conducted on (unpaved) dirt roads inside the UMore Park in Rosemount, Minnesota. Two data runs were performed and the entire route (Figure 3.7) has a total length of 11.1 miles (17.86 km). The weather was mostly sunny and sometimes partly cloudy and the road condition was dry.

Figure 3.7 Route of field evaluation on unpaved dirt roads (Source: Google Maps, ©2012 Google, Sanborn).

Data Analysis

By using the same method described in Section 3.3, results of the speed analysis are shown in Table 3.3 and Figure 3.8 and results of the angle measurement analysis are shown in Table 3.4 and Figure 3.9.

Table 3.3 Results of the speed analysis of ADNS-3080 sensor on dirt roads.

Data run	β (in m/sec)	R-Square
1	0.035594	0.967441
2	0.035084	0.920351

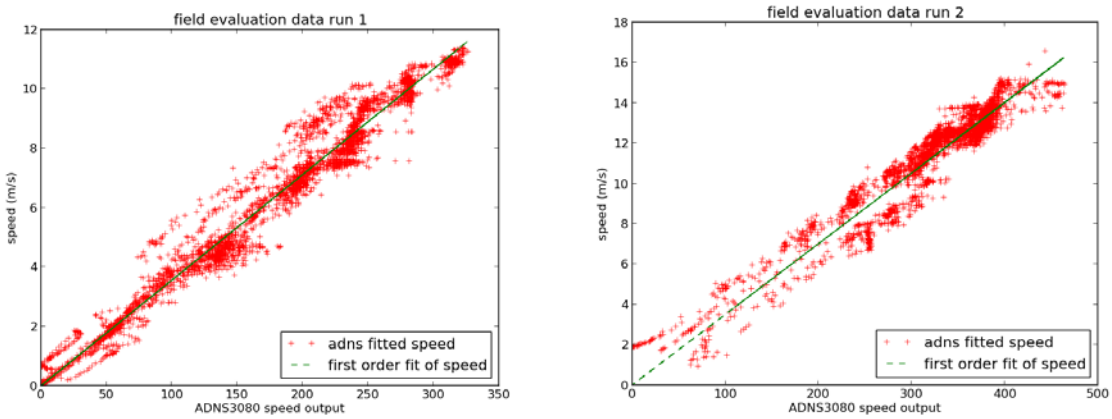

Figure 3.8 Results of field evaluation of ADNS-3080 and fitted speed data on dirt roads.

Table 3.4 Results of the angle analysis of ADNS-3080 sensor on dirt roads.

Data run	Δθ (mean)	Δθ (standard deviation)
1	-3.076189°	2.744785°
2	-2.203083°	2.915702°

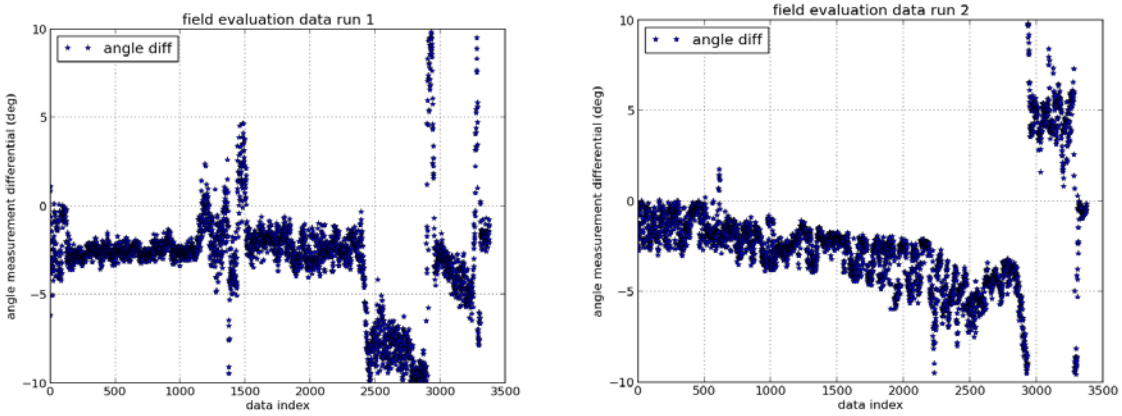

Figure 3.9 Results of field evaluation of ADNS-3080 and angle measurement (differential) data on dirt roads.

3.5 Discussion

Field evaluation of ADNS-3080 mouse sensor showed that speed measurement of the sensor was linear to the speed output of the NovAtel SPAN system. Overall, the mouse sensor had a speed constant β of 0.035, which is consistent with the value found in lab testing. On paved roads, the coefficient of determination (R^2) was greater than 0.98 for both data runs. On dirt roads, the coefficient R-square was greater than 0.92. The results show that ADNS-3080 mouse sensor can be used to compute speeds of a vehicle outside of the lab on real roads.

The results show a much larger variation in angle measurements of ADNS-3080 mouse sensor in the field than in the lab. Also, the ADNS-3080 mouse sensor did worse in angle measurements on dirt roads than on paved roads. The hypothesis is that dirt roads have much different surface texture details than paved roads and the moving roadway in the lab. The moving roadway in the lab has a very homogeneous surface texture, which allows the ADNS-3080 mouse sensor to track easily. Paved roads have either an asphalt or concrete surface and it is common to have both types of surfaces on a single stretch of road. Dirt roads, the most difficult for ADNS-3080 mouse sensor to track of all, have unpredictable surface types with different colors of sand and different types of gravel. With heterogeneous types of surface texture details, the ADNS-3080 mouse sensor had more difficulty to track consistently and reliably, thus the higher degree of error in measurement.

Another factor that affects measurements of ADNS-3080 mouse sensor was the illumination of surface. In an indoor controlled environment like the lab, one halogen lamp was enough to illuminate surface of the moving roadway such that the ADNS-3080 mouse sensor can have high readings of surface quality. High surface quality readings indicate that a high number of surface texture details are visible by the mouse sensor and is key for the ADNS-3080 mouse sensor to track consistently and reliably. Outside of the lab, the illumination is affected by the angle of the sun, shadow of the vehicle (in the sun), etc. The result is inconsistency in illumination and higher variability on surface quality readings and motion tracking. More research is needed to find an optimal light source for the ADNS-3080 mouse sensor to eliminate the sun effect and provide good lighting for the mouse sensor to maintain high surface quality readings.

Chapter 4. Conclusions and Recommendations

4.1 Conclusions

A low-cost speed sensor based on a $5 Avago ADNS-3080 mouse sensor chip was designed and developed to replace the $20,000 Correvit S-350 sensor for GPS augmentation applications. Speed and angle measurements from the velocity sensor are required inputs to the augmentation system to guide a vehicle when GPS signals are not available. Therefore, the replacement velocity sensor needs to be able to measure vehicle speeds and slip angles consistently and reliably.

Key findings of the study include:

1. In-lab testing showed that the ADNS-3080 mouse sensor can consistently and reliably measure speed up to 48 MPH (21.5 m/sec) and angles all around from 0° to 360° using a 17 mm (F4.2) lens.
2. In speed analysis, data showed that the speed output of the ADNS-3080 mouse sensor was linearly proportional to the actual speed measured. The coefficient of determination (R^2) in the linear regression analysis was greater than 0.999 in the lab, and greater than 0.98 on paved roads, and greater than 0.92 on unpaved dirt roads. If measured in m/sec, the mouse sensor had a speed constant (β) of 0.075 when the resolution was set to 400 cpi and a speed constant (β) of 0.035 when the resolution was set to 1600 cpi.
3. In angle measurement analysis, data showed that the ADNS-3080 mouse sensor had a deadband of approximately 20° (±10°) near the X (horizontal) and Y (vertical) axes. This is a feature by design to keep the mouse from drifting to the left or right when the mouse is moved up or down, or vice versa. It helps the mouse move straight lines quickly (either horizontally or vertically) if so desired. To avoid the deadband, the ADNS-3080 mouse sensor was physically rotated 45° in the field sensor box before mounting on a vehicle.
4. Excluding the deadband, the ADNS-3080 mouse sensor was found to have a mean angular measurement error of 1.249° (with a standard deviation of 1.418°) when the sensor was located at 9” (229 mm) above the moving roadway with a 17 mm (F4.2) lens and a resolution of 400 cpi.
5. Several different attempts were made to try to improve the accuracy of angular measurements of ADNS-3080 mouse sensor:
    a. At 400 cpi, the accuracy of the mouse sensor did not improve when the output data rate was modified. Nor was there performance improvement when the mouse sensor was moved closer to the road surface.
    b. Performance of the mouse sensor improved when the resolution was increased from 400 to 1600 cpi. The standard deviation of angular measurements was decreased to 0.135° when the sensor was 4” (102 mm) above the road surface, and 0.236° at 9” (229 mm) above the surface.
    c. The mean angular measurement error did improve when the mouse sensor was moved closer to the road surface at 4” (101.6 mm). However, at this height, the mouse sensor and the illumination lamp could easily be damaged on a moving vehicle. Therefore, the sensor was mounted at 9” (229 mm) above the ground on a vehicle in the field evaluation.

    d. Lenses with longer focal length provided little or no benefit to the mouse sensor. No performance increase was found when the 17 mm lens was replaced with a 25 mm (F2.5) lens. Changing distances between the mouse sensor and the road surface with the 25 mm lens also showed no accuracy improvement over the original configuration of 17 mm lens at 9" (229 mm) above the road surface.
6. Performance of ADNS-3080 mouse sensor in the field was not as consistent as performance observed in the lab.
    a. In speed analysis, it was found that the speed constant (β) remained the same at 0.035. However, the coefficient of determination (R^2) was reduced from 0.999 in the lab to 0.991 on paved roads, and to 0.968 on unpaved dirt roads.
    b. On paved roads, the ADNS-3080 mouse sensor had a mean angle measurement error of -1.747° with a standard deviation of 1.293°. On unpaved dirt roads, the mean error was -2.640° with a standard deviation of 2.830°.

In summary, the ADNS-3080 mouse sensor shows great potential to replace the more expensive Correvit S-350 speed sensor. The speed measurement is consistent and reliable both in the lab and in the field. At 1600 cpi, the angle measurement of ADNS-3080 has a mean error of 1.575° (with a standard deviation of 0.236°) in the lab compared with the accuracy of the Correvit sensor of 0.747° (with a standard deviation of 1.084°). However, the sensor does not do as well in the field and has mean angle error about -2.7° with a larger standard deviation of 2.1°. More research is needed to improve the performance of ADNS-3080 mouse sensor in the field.

4.2 Future Work

The potential of ADNS-3080 mouse sensor to be used as a velocity sensor for DPGS augmentation applications has been explored in this study. Even though the results are promising, it is not ready to be deployed in the field yet. The following recommendations are made to improve the field performance of the sensor:

1. High surface quality readings are a key to consistent and reliable tracking by the ADNS-3080 mouse sensor, and they require good illumination of surface that allows the mouse sensor to detect surface texture details. In the field evaluation, it was found that it is difficult to maintain high surface quality readings under all weather conditions. Depending on the position of the sun in the sky and the direction of vehicle travel, sunlight can cause inconsistency in illumination and higher variability on surface quality readings and motion tracking. More research is needed to find an optimal light source (either single or multiple lamps) to eliminate the sun effect and provide good illumination on the surface so that the mouse sensor can maintain high surface quality readings.
2. Multiple ADNS-3080 mouse sensors can be installed at different locations of a vehicle and a software program can be developed to average and/or filter sensor output. The distance between the mouse sensor and the ground surface varies on a moving vehicle due to rolling and pitching of the vehicle body. This may increase errors in measurement of speed and angle. A multiple-sensor implementation would help to reduce the effect, and thus increase the accuracy of the output.
3. ADNS-3080 is a LED-based mouse sensor. Recently, Avago has introduced laser-based mouse sensors. These new sensors have twice the frame rate (11750 fps) and 4 times the resolution (5670 cpi) than the ADNS-3080 mouse sensor. With much improved

resolution and higher frame rate, the laser-based mouse sensors can measure speeds and angles more accurately. Effort should be invested to develop a prototype to evaluate. With experiences from developing the ADNS-3080 based speed sensor, the time required to create a prototype system can be shortened.

References

1. C. Shankwitz, "Elbow Room on the Shoulder – DGPS-Based Lane-Keeping Enlists Laser Scanners for Safety and Efficiency," *GPS World*, Vol. 21, No. 7 (July 2010), pp 30-37.
2. Corrsys Datron 2-D Non Contact Optical Velocity & Slip Angle Sensors, (Internet, accessed April 2012), http://www.corrsys-datron.com/optical_sensors.htm.
3. E. Arpin, *Evaluation of Correvit S-350 Sensor*, Internal Report, IV Lab, University of Minnesota, Minneapolis, MN, January 2012.
4. Inertial Navigation System, (Internet, accessed April 2012), Wikipedia, http://en.wikipedia.org/wiki/Inertial_navigation_system
5. Optical Flow, (Internet, accessed April 2012), Wikipedia, http://en.wikipedia.org/wiki/Optical_flow
6. J. L. Barron and N. A. Thacker, *Tutorial: Computing 2D and 3D Optical Flow*, Internal report, Medical School, University of Manchester, Manchester, U.K., January 2005.
7. T. Mei, *Understanding Optical Mice*, (Internet, accessed November 2011), March 2010, http://www.avagotech.com/docs/AV02-1265EN
8. D. Flubacher, "*Characterisation of an Optical Flow Sensor for Off-Road Robot Application*," Bachelor thesis, Swiss Federal Institute of Technology, Zurich, Zurich, Switzerland, May 2008.
9. Z. Scheffer, *Optical Speedometer*, Technical report, University of Central Florida, Orlando, FL, April 2007.
10. M. Joos, J. Ziegler, and C. Stiller, "*Low-Cost Sensors for Image Based Measurement of 2D Velocity and Yaw Rate*," 2010 IEEE Intelligent Vehicles Symposium, San Diego, CA, June 2010, pp 658-662.
11. R. Mackay, *Quad Position Hold with Mouse Sensor*, (Internet, accessed October 2011), January 2011, http://www.diydrones.com/profiles/blogs/quad-position-hold-with-mouse-1
12. Sensor Optical Mouse 20-DIP ADNS-3080, (Internet, accessed November 2011), http://parts.digikey.com/1/parts/949059-sensor-optical-mouse-20-dip-adns-3080.html
13. Optical Flow Sensor, (Internet, accessed December 2011), http://store.diydrones.com/ProductDetails.asp?ProductCode=BR-0016-01
14. Navigation Sensors, (Internet, accessed October 2011), http://www.avagotech.com
15. E. Arpin, "*Evaluation of NovAtel SPAN System*," Internal Report, IV Lab, University of Minnesota, Minneapolis, MN, April 2012.

Appendix A: Results of Constant Speed, Constant Angle Tests

Encoder angle	-45.00°	-42.00°	-39.00°	-36.00°	-33.00°	-30.00°	-27.00°	-24.00°	-21.00°	-18.00°	-15.00°
Road speed	β	β	β	β	β	β	β	β	β	β	β
200 (1.23 m/sec)	0.069183	0.069347	0.069018	0.069143	0.06913	0.068781	0.069167	0.068717	0.06879	0.069169	0.068538
350 (2.16 m/sec)	0.069186	0.069336	0.069027	0.069152	0.069263	0.068878	0.0692	0.069329	0.068954	0.069241	0.068456
500 (3.07 m/sec)	0.06912	0.069253	0.068927	0.069173	0.069114	0.069194	0.069148	0.069393	0.06933	0.069434	0.068401
750 (4.61 m/sec)	0.069113	0.069198	0.069077	0.069434	0.069316	0.068771	0.069209	0.069124	0.069368	0.069315	0.068538
1000 (6.14 m/sec)	0.068976	0.068991	0.069051	0.068968	0.069009	0.069046	0.068854	0.068863	0.068902	0.069339	0.06861
1250 (7.63 m/sec)	0.068741	0.068761	0.068978	0.06875	0.068868	0.069029	0.06892	0.069042	0.068889	0.068541	0.068715
1500 (9.27 m/sec)	0.068722	0.068896	0.068531	0.068715	0.069091	0.068975	0.06895	0.069098	0.069097	0.068923	0.068675
1750 (10.83 m/sec)	0.068659	0.068613	0.069239	0.068866	0.068553	0.068852	0.069146	0.068957	0.06901	0.069222	0.069188
2000 (12.28 m/sec)	0.068425	0.068875	0.069162	0.069374	0.068836	0.068505	0.069258	0.069188	0.068859	0.068908	0.069084
2500 (15.43 m/sec)	0.068372	0.069539	0.069401	0.069101	0.06863	0.069404	0.069022	0.068711	0.069896	0.069814	0.069365
3000 (18.50 m/sec)	0.068301	0.069412	0.069414	0.070857	0.070726	0.069926	0.06852	0.068596	0.070365	0.07047	0.069824
3500 (21.57 m/sec)	0.070981	0.070857	0.068226	0.068224	0.068954	0.070905	0.07008	0.069207	0.068882	0.070698	0.070132
Mean (β)	0.068981	0.069256	0.069004	0.069146	0.069124	0.069188	0.069122	0.069018	0.069195	0.069422	0.068960
Std (β)	0.000706	0.000579	0.000337	0.000630	0.000554	0.000649	0.000365	0.000254	0.000482	0.000627	0.000567

Please note that the constant β is for when the road speed is measured in m/sec.

Encoder angle	-12.00°	-9.00°	-6.00°	-3.00°	0.00°	3.00°	6.00°	9.00°	12.00°	15.00°	18.00°
Road speed	β	β	β	β	β	β	β	β	β	β	β
200 (1.23 m/sec)	0.068548	0.069105	0.069273	0.068494	0.068981	0.069621	0.068626	0.068995	0.069333	0.068876	0.069151
350 (2.16 m/sec)	0.06857	0.069113	0.069616	0.068658	0.069121	0.069693	0.068717	0.069012	0.069226	0.068836	0.069185
500 (3.07 m/sec)	0.068673	0.069122	0.069682	0.068566	0.069074	0.069676	0.068698	0.068969	0.069285	0.068894	0.069293
750 (4.61 m/sec)	0.06879	0.069089	0.06932	0.068616	0.069065	0.0697	0.068478	0.068996	0.069411	0.068885	0.069272
1000 (6.14 m/sec)	0.069112	0.069516	0.070189	0.069057	0.069421	0.069944	0.069744	0.069198	0.069666	0.069842	0.068901
1250 (7.63 m/sec)	0.068778	0.069247	0.06889	0.068602	0.069006	0.069742	0.06886	0.068594	0.069091	0.069521	0.068582
1500 (9.27 m/sec)	0.068742	0.068844	0.069282	0.068596	0.069006	0.069765	0.068357	0.068586	0.069463	0.068517	0.068774
1750 (10.83 m/sec)	0.069017	0.069208	0.068889	0.068749	0.069012	0.069679	0.069166	0.068361	0.069083	0.070176	0.070626
2000 (12.28 m/sec)	0.069068	0.069054	0.069786	0.068782	0.069159	0.069842	0.069666	0.068754	0.069637	0.070482	0.068261
2500 (15.43 m/sec)	0.069506	0.070951	0.069585	0.069465	0.069774	0.070513	0.071541	0.07166	0.068404	0.069225	0.070326
3000 (18.50 m/sec)	0.069546	0.070217	0.070131	0.069729	0.069955	0.071052	0.072166	0.068412	0.068977	0.069863	0.070814
3500 (21.57 m/sec)	0.069431	0.069483	0.069967	0.069497	0.069643	0.070519	0.070416	0.068543	0.069584	0.071184	0.072329
Mean (β)	0.068981	0.069412	0.069550	0.068901	0.069268	0.069978	0.069536	0.069006	0.069263	0.069525	0.069626
Std (β)	0.000357	0.000597	0.000434	0.000428	0.000342	0.000459	0.001245	0.000877	0.000351	0.000804	0.001170

Encoder angle	21.00°	24.00°	27.00°	30.00°	33.00°	36.00°	39.00°	42.00°	45.00°		
Road speed	β	β	β	β	β	β	β	β	β	Mean (β)	Std (β)
200 (1.23 m/sec)	0.069253	0.069208	0.06929	0.069072	0.069404	0.06927	0.069383	0.069304	0.069331	0.069081	0.000285
350 (2.16 m/sec)	0.069384	0.069315	0.069337	0.069202	0.069462	0.069331	0.069426	0.069467	0.069489	0.069167	0.000297
500 (3.07 m/sec)	0.069674	0.069444	0.069356	0.069449	0.069554	0.069429	0.069524	0.069487	0.069522	0.069221	0.000329
750 (4.61 m/sec)	0.069861	0.069824	0.0695	0.06944	0.06954	0.069757	0.069567	0.069553	0.069706	0.069253	0.000370
1000 (6.14 m/sec)	0.069101	0.069137	0.069183	0.069378	0.06951	0.06978	0.069605	0.069457	0.06952	0.069286	0.000375
1250 (7.63 m/sec)	0.068838	0.068997	0.069188	0.069334	0.069416	0.069671	0.069623	0.069473	0.069355	0.069034	0.000341
1500 (9.27 m/sec)	0.069641	0.070105	0.069261	0.06951	0.069665	0.06893	0.068818	0.069339	0.06919	0.069034	0.000412
1750 (10.83 m/sec)	0.068852	0.069304	0.069689	0.069463	0.068724	0.069276	0.070046	0.069195	0.069162	0.069161	0.000484
2000 (12.28 m/sec)	0.068952	0.069496	0.069515	0.068344	0.069686	0.07012	0.069452	0.069237	0.068898	0.069183	0.000513
2500 (15.43 m/sec)	0.070563	0.068627	0.069016	0.06982	0.069032	0.069851	0.069995	0.069881	0.068625	0.069600	0.000832
3000 (18.50 m/sec)	0.070797	0.067874	0.068092	0.070927	0.071559	0.071257	0.06962	0.06971	0.069026	0.069875	0.001067
3500 (21.57 m/sec)	0.068882	0.069551	0.070652	0.071547	0.068	0.068155	0.068038	0.072068	0.07181	0.069885	0.001232
3750 (23.14 m/sec)	0.069253	0.069208	0.06929	0.069072	0.069404	0.06927	0.069383	0.069304	0.069331	0.069081	0.000285
4000 (24.66 m/sec)	0.069384	0.069315	0.069337	0.069202	0.069462	0.069331	0.069426	0.069467	0.069489	0.069167	0.000297
Mean (β)	0.069483	0.069240	0.069339	0.069623	0.069462	0.069568	0.069424	0.069680	0.069469		
Std (β)	0.000658	0.000573	0.000573	0.000842	0.000819	0.000737	0.000534	0.000776	0.000796		

Appendix B: Angular Measurements of ADNS-3080 Sensor

Encoder angle	-45.00°	-42.00°	-39.00°	-36.00°	-33.00°	-30.00°	-27.00°	-24.00°	-21.00°	-18.00°
Road speed	θ	θ	θ	θ	θ	θ	θ	θ	θ	θ
200 (1.23 m/sec)	-43.569°	-39.656°	-37.286°	-33.589°	-31.524°	-27.366°	-25.189°	-22.083°	-18.483°	-16.453°
350 (2.16 m/sec)	-43.461°	-39.724°	-37.273°	-33.669°	-31.53°	-27.488°	-25.14°	-22.263°	-18.538°	-16.377°
500 (3.07 m/sec)	-43.253°	-39.784°	-36.821°	-33.689°	-31.4°	-27.33°	-25.18°	-22.324°	-18.643°	-16.345°
750 (4.61 m/sec)	-43.287°	-39.882°	-37.333°	-34.056°	-31.492°	-27.848°	-25.659°	-22.089°	-18.795°	-16.416°
1000 (6.14 m/sec)	-43.372°	-39.962°	-37.381°	-35.034°	-31.676°	-27.674°	-25.074°	-22.176°	-19.445°	-16.776°
1250 (7.63 m/sec)	-43.539°	-40.055°	-37.361°	-34.862°	-31.595°	-27.836°	-25.254°	-22.559°	-19.338°	-15.959°
1500 (9.27 m/sec)	-43.415°	-40.22°	-37.51°	-34.149°	-31.067°	-28.552°	-25.818°	-22.113°	-18.926°	-16.395°
1750 (10.83 m/sec)	-43.526°	-40.386°	-37.306°	-34.377°	-31.457°	-28.216°	-25.228°	-22.699°	-19.83°	-16.131°
2000 (12.28 m/sec)	-43.446°	-40.342°	-37.259°	-34.341°	-31.453°	-28.626°	-25.275°	-22.146°	-19.561°	-16.659°
2500 (15.43 m/sec)	-43.494°	-40.765°	-37.391°	-34.194°	-31.566°	-28.497°	-25.418°	-22.407°	-19.066°	-16.367°
3000 (18.50 m/sec)	-43.473°	-40.683°	-37.263°	-34.46°	-30.982°	-27.74°	-25.951°	-22.92°	-19.476°	-16.209°
3500 (21.57 m/sec)	-43.475°	-39.509°	-38.156°	-34.663°	-31.557°	-28.861°	-25.396°	-22.282°	-19.322°	-16.068°

Encoder angle	-15.00°	-12.00°	-9.00°	-6.00°	-3.00°	0.00°	3.00°	6.00°	9.00°	12.00°
Road speed	θ	θ	θ	θ	θ	θ	θ	θ	θ	θ
200 (1.23 m/sec)	-12.994°	-9.577°	-8.766°	-4.751°	-0.001°	0°	0.001°	6.297°	9.127°	13.21°
350 (2.16 m/sec)	-12.871°	-9.597°	-8.748°	-5.116°	0°	0°	0°	6.286°	9.118°	13.287°
500 (3.07 m/sec)	-12.722°	-9.56°	-8.671°	-5.121°	0°	0°	0°	6.167°	9.138°	13.339°
750 (4.61 m/sec)	-12.827°	-9.613°	-8.701°	-4.607°	0°	0°	0°	5.77°	9.149°	13.369°
1000 (6.14 m/sec)	-12.937°	-10.352°	-9.426°	-4.653°	0°	0°	0°	3.259°	9.042°	13.2°
1250 (7.63 m/sec)	-12.575°	-10.059°	-9.052°	-1.238°	0°	0°	0°	3.179°	9.336°	13.455°
1500 (9.27 m/sec)	-13.183°	-9.848°	-8.803°	-4.984°	0°	0°	0°	6.127°	9.187°	13.452°
1750 (10.83 m/sec)	-12.965°	-10.584°	-9.443°	-0.842°	0°	0°	0°	2.98°	9.849°	13.496°
2000 (12.28 m/sec)	-13°	-10.255°	-9.281°	-4.123°	0°	0°	0°	2.993°	8.932°	13.079°
2500 (15.43 m/sec)	-13.947°	-11.106°	-3.719°	-0.002°	0°	0°	0°	0.198°	2.381°	12.959°
3000 (18.50 m/sec)	-13.372°	-10.969°	-8.905°	-0.015°	0°	0°	0°	0.058°	9.359°	13.984°
3500 (21.57 m/sec)	-12.99°	-10.731°	-9.633°	-1.371°	0°	0°	0°	2.728°	10.21°	13.213°

Encoder angle	15.00°	18.00°	21.00°	24.00°	27.00°	30.00°	33.00°	36.00°	39.00°	42.00°	45.00°
Road speed	θ	θ	θ	θ	θ	θ	θ	θ	θ	θ	θ
200 (1.23 m/sec)	16.56°	19.459°	22.149°	25.536°	28.27°	30.992°	34.528°	36.908°	40.432°	42.839°	46.519°
350 (2.16 m/sec)	16.501°	19.529°	22.211°	25.503°	28.3°	31.103°	34.506°	36.997°	40.362°	42.907°	46.546°
500 (3.07 m/sec)	16.496°	19.613°	22.312°	25.594°	28.323°	31.087°	34.547°	37.057°	40.238°	42.985°	46.702°
750 (4.61 m/sec)	16.554°	19.695°	22.282°	25.465°	28.462°	31.301°	34.472°	37.482°	40.568°	43.161°	46.728°
1000 (6.14 m/sec)	16.233°	19.523°	22.462°	25.492°	28.436°	31.412°	34.732°	37.682°	40.464°	43.291°	46.639°
1250 (7.63 m/sec)	16.457°	19.612°	22.74°	25.494°	28.496°	31.569°	34.647°	37.507°	40.475°	43.389°	46.485°
1500 (9.27 m/sec)	16.671°	19.808°	22.183°	25.225°	28.212°	31.351°	34.521°	37.418°	40.571°	43.583°	46.558°
1750 (10.83 m/sec)	15.477°	18.882°	21.985°	25.063°	28.275°	31.586°	34.484°	37.645°	40.453°	43.298°	46.483°
2000 (12.28 m/sec)	16.32°	19.39°	22.585°	25.827°	28.717°	31.815°	33.787°	37.169°	40.344°	43.73°	46.552°
2500 (15.43 m/sec)	16.059°	18.987°	22.51°	25.317°	28.592°	32.031°	34.697°	36.828°	40.541°	44.093°	46.518°
3000 (18.50 m/sec)	16.867°	20.155°	22.102°	26.184°	29.486°	29.791°	33.686°	37.62°	40.182°	44.148°	46.529°
3500 (21.57 m/sec)	15.186°	18.856°	21.767°	24.77°	28.516°	32.462°	34.176°	37.743°	41.635°	42.011°	46.497°

Appendix C: Results of Linear Speed Tests of ADNS-3080 Sensor

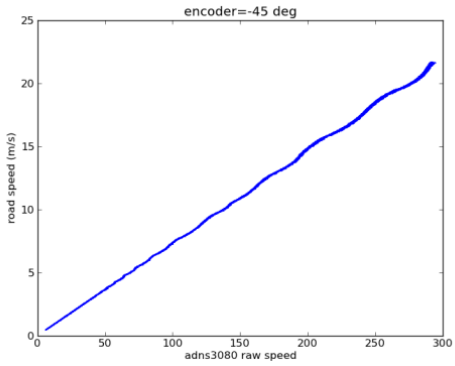
encoder=-45 deg
road speed (m/s)
adns3080 raw speed

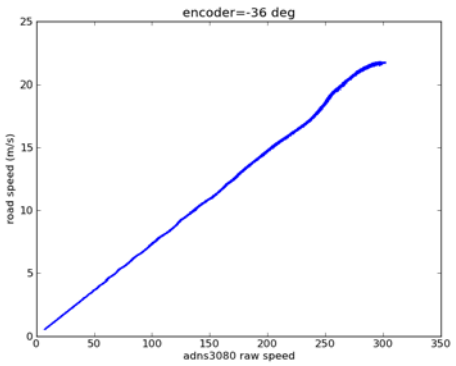
encoder=-36 deg
road speed (m/s)
adns3080 raw speed

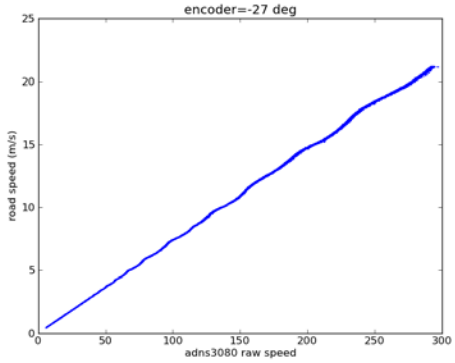
encoder=-27 deg
road speed (m/s)
adns3080 raw speed

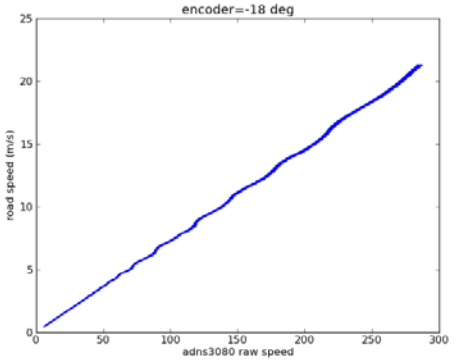
encoder=-18 deg
road speed (m/s)
adns3080 raw speed

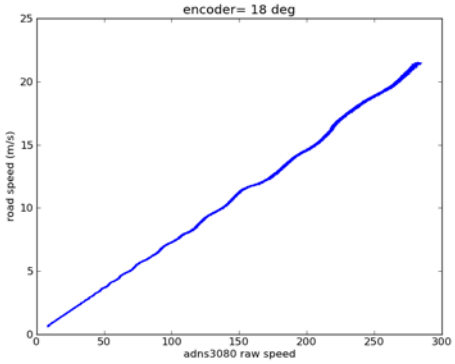
encoder= 18 deg
road speed (m/s)
adns3080 raw speed

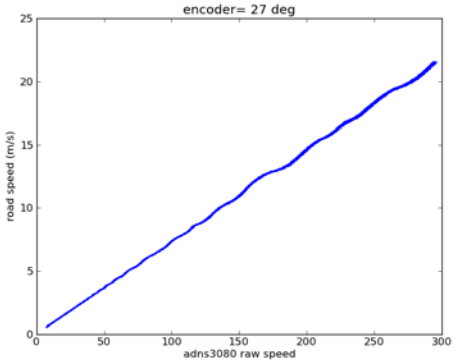
encoder= 27 deg
road speed (m/s)
adns3080 raw speed

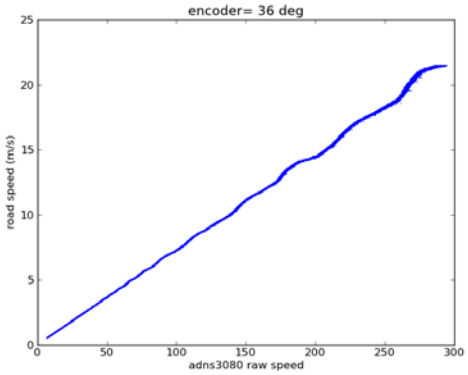
encoder= 36 deg
road speed (m/s)
adns3080 raw speed

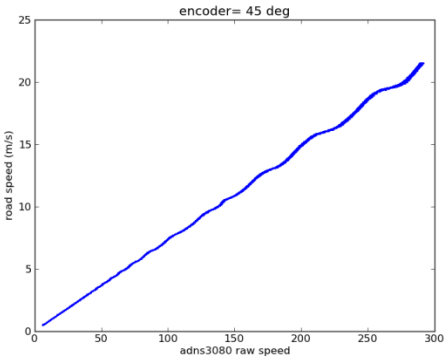
encoder= 45 deg
road speed (m/s)
adns3080 raw speed

Appendix D: Results of Angle Measurements at Different Moving Roadway Speeds

	rpm = 750		rpm = 1500		rpm = 2500	
Encoder Angle (°)	**Angle differential (mean, °)**	**Angle differential (std, °)**	**Angle differential (mean, °)**	**Angle differential (std, °)**	**Angle differential (mean, °)**	**Angle differential (std, °)**
-168	0.419126	0.190788	0.316786	0.12801	2.246273	0.052675
-165	1.885176	0.152285	1.766905	0.097588	2.009699	0.042578
-162	1.88849	0.167089	1.610501	0.082786	1.452432	0.04731
-159	1.24527	0.129076	1.129213	0.067861	1.695598	0.054803
-156	1.337196	0.115258	1.423984	0.066025	1.948257	0.044254
-153	0.91813	0.121223	1.60562	0.061215	1.465125	0.075642
-150	0.806426	0.146237	1.375355	0.057138	1.101312	0.04935
-147	2.167234	0.152957	1.190174	0.075608	1.610821	0.055206
-144	1.611846	0.118476	1.281286	0.074519	1.463736	0.041496
-141	1.158254	0.116437	1.381649	0.068367	1.607241	0.049769
-138	1.107197	0.159125	1.201785	0.088111	1.081268	0.059803
-135	1.753271	0.263124	1.838014	0.07779	1.952899	0.060243
-132	1.376649	0.104171	1.403087	0.057986	1.404803	0.044312
-129	1.452418	0.135812	1.462738	0.081412	1.25215	0.041268
-126	1.09235	0.166861	2.245393	0.081489	1.366612	0.051227
-123	2.595093	0.176676	1.511268	0.060506	1.866869	0.049399
-120	2.529598	0.13871	0.866391	0.062427	1.496825	0.058253
-117	1.146309	0.121882	1.686921	0.073786	0.879636	0.042879
-114	1.311389	0.129256	1.869156	0.068375	1.706823	0.048593
-111	1.132411	0.161146	0.611872	0.076526	1.771046	0.044205
-108	0.192721	0.165768	0.51298	0.102454	0.713405	0.051477
-105	3.038157	0.187888	2.700776	0.104023	1.310344	0.086532
-102	2.122385	0.141831	1.96695	0.08057	2.114202	0.109244
-78	0.559448	0.181244	0.428523	0.098565	1.714835	0.062201
-75	1.857097	0.148429	1.604767	0.078988	1.911494	0.042295
-72	1.444269	0.135295	1.806288	0.081385	1.337176	0.044017
-69	1.513636	0.115386	1.198432	0.071113	1.497596	0.047146
-66	1.607838	0.110807	1.327248	0.07264	1.912368	0.044547
-63	0.650093	0.129434	1.697304	0.062001	1.331242	0.075141
-60	0.613063	0.179201	1.315421	0.069307	1.192104	0.046739
-57	1.529992	0.12869	0.924693	0.092402	1.67993	0.049267
-54	1.313911	0.137972	1.354025	0.074634	1.546692	0.040008
-51	1.214419	0.111648	1.320978	0.066951	1.350349	0.047094
-48	1.76817	0.143947	1.241207	0.089048	1.053637	0.064445
-45	1.10209	0.159586	1.672701	0.065927	1.908401	0.05788
-42	1.388791	0.112951	1.281405	0.070017	1.437843	0.046376
-39	1.286082	0.14675	1.405715	0.084205	1.151288	0.041337
-36	1.067004	0.190834	2.168329	0.081867	1.309596	0.051726
-33	2.511621	0.185535	1.391602	0.06062	1.81691	0.047266
-30	2.506079	0.132368	0.83176	0.064401	1.516261	0.059738
-27	1.060729	0.131504	1.66543	0.070023	0.692397	0.047003

	rpm = 750		rpm = 1500		rpm = 2500	
Encoder Angle (°)	**Angle differential (mean, °)**	**Angle differential (std, °)**	**Angle differential (mean, °)**	**Angle differential (std, °)**	**Angle differential (mean, °)**	**Angle differential (std, °)**
-24	1.31158	0.136738	1.896513	0.071042	1.505113	0.056197
-21	1.184348	0.205545	0.679259	0.081553	1.670306	0.045769
-18	0.279927	0.15127	0.661818	0.082056	0.651521	0.050047
-15	2.733426	0.201848	2.528262	0.106629	0.80437	0.098406
-12	1.869666	0.163655	1.708085	0.087247	1.883823	0.122631
12	0.238513	0.227512	0.11813	0.150777	1.922962	0.053395
15	1.557062	0.158296	1.690733	0.107264	1.759717	0.04362
18	1.396735	0.154424	1.240604	0.096377	1.45829	0.043876
21	1.366242	0.125126	0.914206	0.086111	1.614316	0.08074
24	1.553857	0.117856	1.454626	0.070787	1.962674	0.042609
27	0.965961	0.127359	1.358691	0.066757	1.524789	0.103017
30	0.939469	0.14808	1.484614	0.076106	0.908695	0.052471
33	1.453925	0.132621	1.734319	0.092919	1.743719	0.066687
36	1.274945	0.11948	1.159308	0.06843	1.114594	0.041312
39	1.236919	0.103843	1.48776	0.064813	2.036307	0.044992
42	1.210014	0.144953	0.94828	0.074886	0.563668	0.068046
45	1.816721	0.132384	1.806937	0.074435	2.144372	0.056348
48	1.409422	0.126181	1.207199	0.088463	0.66139	0.040837
51	1.265445	0.113156	1.674424	0.075189	1.499496	0.044616
54	0.675018	0.138363	1.324287	0.083145	1.372716	0.082605
57	1.878376	0.145222	1.173272	0.067226	1.756794	0.044539
60	1.878997	0.146851	1.168617	0.06704	1.620657	0.090147
63	1.461285	0.154401	1.289117	0.078355	0.61933	0.044189
66	1.880701	0.124834	1.908214	0.063904	1.520531	0.088483
69	0.60692	0.139737	1.140626	0.086748	1.345834	0.047872
72	0.411565	0.160866	0.821325	0.088896	0.762754	0.042782
75	2.842315	0.181016	2.630287	0.126926	0.298212	0.052786
78	2.061381	0.182289	1.801688	0.093712	2.518154	0.163237
102	0.053081	0.264611	-0.231287	0.15429	1.769991	0.040539
105	1.590462	0.152932	2.162007	0.120978	1.634333	0.041737
108	1.412211	0.155661	1.015532	0.089509	1.572836	0.051053
111	1.017698	0.146818	0.860926	0.091077	1.266965	0.105547
114	1.341041	0.116492	1.596704	0.082898	2.029766	0.042849
117	1.128712	0.108861	1.228495	0.064655	1.377098	0.103608
120	1.070665	0.135339	1.572832	0.070616	0.922017	0.053717
123	1.543866	0.134003	1.922541	0.097406	1.873072	0.077721
126	1.330469	0.118158	1.03455	0.073281	1.111968	0.046619
129	1.319866	0.118512	1.475394	0.079113	2.148509	0.046449
132	1.221117	0.139662	0.963139	0.080945	0.567479	0.062556
135	1.69719	0.139239	1.866364	0.075823	2.218526	0.057928
138	1.314348	0.122521	1.277971	0.078164	0.733822	0.047638
141	1.335661	0.131148	1.69389	0.074878	1.492289	0.044629

	rpm = 750		rpm = 1500		rpm = 2500	
Encoder Angle (°)	**Angle differential (mean, °)**	**Angle differential (std, °)**	**Angle differential (mean, °)**	**Encoder Angle (°)**	**Angle differential (mean, °)**	**Angle differential (std, °)**
144	0.701144	0.157033	1.39807	0.080387	1.318656	0.083064
147	2.023475	0.150234	1.229048	0.0602	1.782435	0.04425
150	1.997272	0.141419	1.098991	0.07073	1.678841	0.079138
153	1.495282	0.147192	1.401316	0.073031	0.631735	0.040868
156	1.830222	0.125068	1.892736	0.076025	1.44272	0.07672
159	0.461459	0.140478	0.920074	0.086874	1.434424	0.044103
162	0.351235	0.163576	0.745187	0.087523	0.494326	0.050076
165	2.490532	0.185977	2.422534	0.117361	0.002822	0.067807
168	1.652815	0.157754	1.69574	0.087815	2.024407	0.164559
overall	1.395891	0.030199	1.389658	0.018140	1.441865	0.024061

Appendix E: Results of Angle Measurements at 1º Increment and Different Data Output Rate

Data rate	100Hz						20Hz					
speed	rpm = 750		rpm = 1550		rpm = 2500		rpm = 750		rpm = 1550		rpm = 2500	
Encoder Angle (°)	Angle differential (mean, °)	Angle differential (std, °)	Angle differential (mean, °)	Angle differential (std, °)	Angle differential (mean, °)	Angle differential (std, °)	Angle differential (mean, °)	Angle differential (std, °)	Angle differential (mean, °)	Angle differential (std, °)	Angle differential (mean, °)	Angle differential (std, °)
-130	1.236179	0.407608	1.322316	0.230732	1.297503	0.137676	1.273725	0.115642	1.277983	0.069848	1.298908	0.038055
-129	1.420968	0.440054	1.50093	0.252314	1.251282	0.143848	1.410016	0.143582	1.467222	0.07653	1.246895	0.037146
-128	1.744917	0.45369	1.661382	0.278886	1.311285	0.166482	1.658738	0.156645	1.679381	0.094156	1.309223	0.041866
-127	1.593814	0.48913	2.048295	0.328053	1.467954	0.192348	1.418836	0.156936	2.107343	0.094595	1.466844	0.047467
-126	1.087594	0.508746	2.236852	0.30334	1.374662	0.163609	0.886607	0.168867	2.211544	0.08448	1.369392	0.053417
-125	0.836224	0.519719	2.115909	0.266334	1.267836	0.171853	0.678687	0.182655	2.078752	0.0747	1.267039	0.04782
-124	1.524705	0.528189	1.846809	0.23496	1.616767	0.164611	1.525239	0.183652	1.808773	0.070199	1.618041	0.046854
-123	2.628151	0.573155	1.487691	0.217538	1.857158	0.159679	2.582342	0.176002	1.481157	0.065526	1.869339	0.0509
-122	2.982458	0.554861	1.154707	0.220542	1.933903	0.163212	2.927446	0.169237	1.155679	0.058456	1.946759	0.049643
-121	2.889857	0.515365	0.938322	0.234967	1.848535	0.170095	2.887691	0.141812	0.944583	0.062489	1.853871	0.050755
-120	2.517585	0.492399	0.907193	0.241984	1.485715	0.164979	2.554089	0.134669	0.904225	0.063246	1.480071	0.05906
-119	1.993441	0.457336	1.087108	0.258401	1.042869	0.167827	2.041272	0.114803	1.070402	0.063457	1.050867	0.057946
-118	1.489734	0.446451	1.427639	0.24395	0.85852	0.154889	1.496713	0.112913	1.391584	0.062603	0.869462	0.049129
-117	1.168291	0.471908	1.815625	0.256023	0.882652	0.143736	1.148137	0.123084	1.76315	0.069593	0.879277	0.042437
-116	1.027261	0.469088	2.066921	0.26466	1.116212	0.145863	0.999773	0.133062	2.025048	0.067791	1.122502	0.040602
-115	1.128997	0.47561	2.083964	0.263289	1.480743	0.161216	1.003874	0.137026	2.067981	0.066496	1.486764	0.056458
-114	1.617928	0.459023	1.854622	0.245928	1.709574	0.178512	1.292016	0.126163	1.863479	0.064393	1.716242	0.053231
-113	1.955379	0.472683	1.452464	0.250454	1.974269	0.174989	1.624247	0.124531	1.470349	0.062043	1.972699	0.048017
-112	1.968475	0.510163	0.984075	0.269205	1.997502	0.164142	1.562117	0.137831	0.998807	0.066094	2.000939	0.046593
-111	1.152194	0.565199	0.570856	0.280558	1.770148	0.152399	1.045203	0.174221	0.572012	0.06653	1.777288	0.041008
-110	1.021823	0.517672	0.300783	0.305904	1.367942	0.135976	0.811735	0.293756	0.297462	0.073939	1.375077	0.039414
mean	1.665998	0.4918118	1.469736	0.259429	1.472049	0.160854	1.563262	0.152718	1.458900	0.070341	1.475119	0.047515

Appendix F: Results of Angle Measurements at 4” above the Moving Roadway

	Data rate = 100 Hz, sensor resolution = 400 cpi, distance to moving roadway = 4”					
speed	**rpm = 750**		**rpm = 1500**		**rpm = 2500**	
Encoder Angle (°)	**Angle differential (mean, °)**	**Angle differential (std, °)**	**Angle differential (mean, °)**	**Angle differential (std, °)**	**Angle differential (mean, °)**	**Angle differential (std, °)**
-130	1.541557	0.203939	2.411891	0.155641	1.719912	0.142378
-129	1.800926	0.251928	2.117808	0.126247	1.904759	0.163493
-128	0.891883	0.349723	1.785665	0.115345	1.899561	0.14077
-127	0.784497	0.388605	1.428832	0.114118	1.753176	0.098111
-126	1.582222	0.362461	1.072565	0.130452	1.710695	0.160041
-125	2.127623	0.275179	0.724809	0.157566	1.895505	0.191839
-124	2.33641	0.253631	0.461976	0.215802	2.119836	0.13032
-123	2.137431	0.243489	0.540695	0.321312	2.081745	0.107098
-122	1.575797	0.275472	1.145035	0.386822	1.982609	0.125736
-121	1.039815	0.244651	1.935755	0.237647	1.770794	0.126211
-120	1.053807	0.22046	2.267388	0.310398	1.536306	0.11571
-119	1.233489	0.211708	2.035681	0.40779	1.337693	0.126329
-118	1.426742	0.210126	1.671241	0.454087	1.367161	0.185176
-117	1.641773	0.237903	1.510118	0.560646	2.07484	0.27423
-116	1.754044	0.296479	1.112025	0.48933	2.65854	0.365086
-115	1.564242	0.390954	1.04617	0.578324	2.552298	0.403061
-114	1.169234	0.370059	0.82721	0.54687	2.406347	0.412174
-113	1.061834	0.282201	0.651617	0.508815	2.269622	0.359706
-112	1.031034	0.240498	0.676889	0.459332	2.078187	0.280259
-111	1.00635	0.217554	1.883444	0.423992	2.204064	0.226124
-110	1.072803	0.213949	3.729888	0.263314	3.067653	0.225104
mean	1.420643	0.273379	1.477938	0.331611	2.018633	0.207569

Appendix G: Results of Angle Measurements at 1600 cpi Sensor Resolution

	Data rate = 100 Hz, sensor resolution = 1600 cpi, distance to moving roadway = 4”					
speed	**rpm = 750**		**rpm = 1500**		**rpm = 2500**	
Encoder Angle (°)	**Angle differential (mean, °)**	**Angle differential (std, °)**	**Angle differential (mean, °)**	**Angle differential (std, °)**	**Angle differential (mean, °)**	**Angle differential (std, °)**
-130	1.205457	0.128749	0.118044	0.193532	1.69658	0.065318
-129	1.302883	0.144569	0.511137	0.154059	2.223409	0.066536
-128	1.308537	0.175065	0.801393	0.117335	1.53757	0.151395
-127	1.094434	0.201876	1.006692	0.103195	-0.029215	0.159214
-126	1.137495	0.188083	1.1979	0.101223	0.39496	0.151542
-125	1.189665	0.143512	1.418235	0.117044	1.067133	0.111716
-124	1.171713	0.122937	1.222267	0.199772	1.756626	0.095713
-123	1.135617	0.12141	-0.116351	0.171208	1.593197	0.203241
-122	1.135366	0.140724	-0.247882	0.206018	0.131293	0.124093
-121	1.076157	0.171069	-0.026334	0.188848	0.397833	0.104604
-120	1.039202	0.161152	0.241711	0.17624	0.799054	0.069106
-119	1.088159	0.14304	0.534697	0.159988	1.10789	0.061805
-118	1.205939	0.13712	0.879391	0.144219	1.19226	0.096246
-117	1.352191	0.138172	1.247326	0.126437	0.285174	0.107653
-116	1.417527	0.141716	1.533157	0.112671	0.100432	0.123224
-115	1.421533	0.151221	1.691372	0.109608	0.388393	0.127468
-114	1.379069	0.161807	1.729795	0.114474	0.853501	0.117482
-113	1.310189	0.17537	1.729741	0.117804	1.267635	0.090415
-112	1.226326	0.185599	1.62682	0.11292	1.456708	0.072979
-111	1.164298	0.186938	1.35427	0.096367	1.292523	0.085469
-110	1.234432	0.182049	1.243474	0.099471	0.83413	0.10147
mean	1.218866	0.157246	0.937945	0.139163	0.968908	0.108889

Appendix H: Results of Angle Measurements at 1600 cpi Sensor Resolution, Height at 9”

	Data rate = 100 Hz, sensor resolution = 1600 cpi, distance to moving roadway = 9”					
speed	**rpm = 750**		**rpm = 1500**		**rpm = 2500**	
Encoder Angle (°)	**Angle differential (mean, °)**	**Angle differential (std, °)**	**Angle differential (mean, °)**	**Angle differential (std, °)**	**Angle differential (mean, °)**	**Angle differential (std, °)**
-130	1.671973	0.392019	1.266848	0.18382	1.253005	0.102267
-129	1.983489	0.400823	1.535777	0.22656	1.102943	0.106208
-128	2.246052	0.346795	1.849895	0.263076	1.057295	0.131744
-127	2.139946	0.312888	2.090254	0.30016	1.114934	0.152494
-126	1.782401	0.293265	2.294331	0.298648	1.179149	0.127608
-125	1.293511	0.305392	2.183215	0.267234	1.384162	0.125664
-124	1.285692	0.4099	1.866405	0.214985	1.544584	0.105798
-123	2.656998	0.554332	1.547736	0.169294	1.566012	0.101081
-122	2.990222	0.522943	1.225442	0.145494	1.459792	0.113733
-121	2.855493	0.442547	0.992611	0.148548	1.273159	0.130921
-120	2.48514	0.37184	0.909034	0.167577	1.078535	0.156785
-119	2.013096	0.342659	1.047253	0.198655	0.950097	0.160016
-118	1.580291	0.33161	1.581991	0.197622	0.877993	0.138983
-117	1.251883	0.330481	1.968297	0.207656	0.901901	0.125722
-116	1.054615	0.326209	2.07326	0.201412	1.196986	0.137971
-115	1.197119	0.332179	1.946768	0.170611	1.751801	0.18485
-114	1.814439	0.360571	1.665635	0.15743	2.059766	0.205983
-113	2.110064	0.326345	1.232131	0.14434	2.201267	0.200097
-112	2.131205	0.336198	0.742069	0.164665	2.121797	0.17744
-111	1.788287	0.333272	0.305953	0.187277	1.831215	0.145718
-110	1.246259	0.319215	0.021085	0.233108	1.402815	0.116757
mean	1.884675	0.366261	1.445047	0.202293	1.395676	0.140373

Appendix I: Results of Angle Measurements at 1600 cpi Sensor Resolution, Height at 9” with 25 mm Lens

25 mm lens	Data rate = 100 Hz, sensor resolution = 1600 cpi, distance to moving roadway = 9”					
speed	rpm = 750		rpm = 1500		rpm = 2500	
Encoder Angle (°)	Angle differential (mean, °)	Angle differential (std, °)	Angle differential (mean, °)	Angle differential (std, °)	Angle differential (mean, °)	Angle differential (std, °)
-130	1.159929	0.727603	0.567835	0.204363	-0.945822	0.339429
-129	3.726235	0.44482	0.579783	0.431776	-0.291721	0.536244
-128	4.318326	0.303348	2.622254	0.654946	2.611029	0.573503
-127	4.196488	0.271631	4.006539	0.283864	3.892898	0.242754
-126	3.760698	0.261297	3.718607	0.166717	3.636972	0.139192
-125	3.21091	0.212374	3.179375	0.154262	3.111291	0.119968
-124	2.555524	0.183892	2.5431	0.137253	2.493941	0.111958
-123	1.821778	0.203948	1.825099	0.125126	1.806311	0.125948
-122	1.055805	0.206879	1.07867	0.12273	1.0953	0.132857
-121	0.307468	0.230626	0.361024	0.138294	0.393333	0.117281
-120	0.016704	0.444796	-0.304524	0.153051	-0.250026	0.11919
-119	0.52707	0.610568	-0.861259	0.171513	-0.787847	0.131221
-118	1.304819	0.620615	-1.265976	0.185976	-1.12334	0.163492
-117	1.987201	0.597835	-0.653877	0.490563	-0.322236	0.531696
-116	3.300572	0.4892	2.811067	0.525317	2.963295	0.430155
-115	3.2632	0.45219	3.306145	0.456871	3.647201	0.363889
-114	2.710351	0.458951	2.907845	0.46095	3.150245	0.444595
-113	2.042392	0.464984	2.121709	0.5018	2.941699	0.41436
-112	1.637748	0.513727	1.318086	0.71141	2.05465	0.668382
-111	0.684251	0.477955	0.68056	0.768707	1.33003	0.557966
-110	-0.269058	0.512847	-0.314153	0.392147	0.117094	0.498572
mean	2.062781	0.413813	1.439424	0.344649	1.501157	0.322031

Appendix J: Results of Angle Measurements at 1600 cpi Sensor Resolution, Height at 4” with 17 mm Lens

17mm lens	Data rate = 100 Hz, sensor resolution = 1600 cpi, distance to moving roadway = 4”									
speed	rpm = 350		rpm = 750		rpm = 1000		rpm = 1200		rpm = 1500	
Encoder Angle (°)	Angle differential (mean, °)	Angle differential (std, °)	Angle differential (mean, °)	Angle differential (std, °)	Angle differential (mean, °)	Angle differential (std, °)	Angle differential (mean, °)	Angle differential (std, °)	Angle differential (mean, °)	Angle differential (std, °)
-130	1.164274	0.217822	1.227503	0.134332	1.024845	0.127988	1.551713	0.095575	-0.895658	0.102091
-129	1.070297	0.234547	1.133186	0.145776	1.227599	0.119945	2.155615	0.092142	-0.305763	0.097862
-128	1.013346	0.268016	0.97249	0.171094	1.398334	0.123849	1.268371	0.18891	0.401095	0.107587
-127	0.977474	0.297983	0.951343	0.167112	1.537373	0.141431	0.549911	0.127696	1.063073	0.114893
-126	0.867142	0.314686	1.037469	0.147128	1.431357	0.130612	1.204494	0.129579	1.657421	0.101879
-125	0.793003	0.363281	1.179577	0.128746	1.103942	0.13942	1.76484	0.121267	2.207162	0.099106
-124	1.1324	0.386004	1.226967	0.128174	1.188486	0.116952	2.473772	0.116458	2.575476	0.110532
-123	1.861781	0.319288	1.267529	0.143309	1.214007	0.102256	3.057454	0.113998	0.668001	0.187825
-122	1.803635	0.273636	1.396189	0.158714	1.218883	0.109664	3.522352	0.116818	-0.330654	0.120047
-121	1.696602	0.259886	1.357987	0.126939	1.277691	0.129079	3.776293	0.132827	0.184479	0.120556
-120	1.631226	0.258408	1.258156	0.114764	1.273381	0.142196	3.846874	0.170919	0.754464	0.1219
-119	1.628822	0.275372	1.184715	0.112239	1.270098	0.145884	1.994259	0.448997	1.341006	0.120564
-118	1.755808	0.263902	1.139814	0.127031	1.287722	0.128919	-0.891657	0.478995	1.958126	0.127562
-117	1.700641	0.248857	1.14605	0.150017	1.240821	0.109584	-1.085596	0.348129	2.539462	0.128531
-116	1.528254	0.233111	1.16938	0.174396	1.159721	0.10655	-0.30011	0.351526	2.955522	0.121335
-115	1.375432	0.223675	1.170247	0.189562	1.215304	0.120052	0.548403	0.338519	3.20663	0.122167
-114	1.305208	0.230283	1.133857	0.193281	1.224723	0.123234	1.938861	0.565466	2.325549	0.312805
-113	1.232598	0.249854	1.066291	0.201504	1.204491	0.120566	2.76168	0.377378	-0.766082	0.397769
-112	1.188358	0.257421	0.966302	0.208259	1.183962	0.114312	3.595559	0.346505	-1.652001	0.18644
-111	1.119448	0.256355	0.852217	0.220378	1.201523	0.113563	4.289587	0.40578	-0.94913	0.207025
-110	1.000023	0.262379	1.184015	0.222569	1.284491	0.119792	3.376138	0.584049	0.095095	0.325816
mean	1.326	0.271	1.144	0.160	1.246	0.123	1.971	0.269	0.906	0.159

Appendix K: Results of Angle Measurements at 1600 cpi Sensor Resolution, Height at 6” with 25 mm Lens

25mm lens	Data rate = 100 Hz, sensor resolution = 1600 cpi, distance to moving roadway = 6”							
speed	rpm = 350		rpm = 750		rpm = 1000		rpm = 1500	
Encoder Angle (°)	Angle differential (mean, °)	Angle differential (std, °)	Angle differential (mean, °)	Angle differential (std, °)	Angle differential (mean, °)	Angle differential (std, °)	Angle differential (mean, °)	Angle differential (std, °)
-130	0.805669	0.418193	3.174505	0.203815	1.157648	0.08455	1.791453	0.072274
-129	0.216624	0.380639	2.896857	0.143605	0.659442	0.092079	1.367032	0.067703
-128	0.036481	0.47971	2.52416	0.130621	0.138532	0.112292	0.871978	0.076021
-127	1.042002	0.868994	2.140461	0.125646	-0.385299	0.126752	0.373837	0.082964
-126	1.331968	0.763633	1.730091	0.124161	-0.517824	0.320697	-0.096032	0.098745
-125	1.1717	0.687002	1.384959	0.183339	1.456064	1.011079	-0.458525	0.140258
-124	1.291623	0.804042	2.016576	0.404684	2.853551	0.244377	0.457812	0.303134
-123	3.067234	0.541795	3.326005	0.237174	2.54922	0.237279	2.619595	0.27209
-122	3.144198	0.23725	3.111848	0.122312	2.258644	0.258069	3.006169	0.093362
-121	2.740539	0.238782	2.68947	0.09845	2.072529	0.327398	2.619596	0.072079
-120	2.377671	0.281691	2.20015	0.093327	2.311631	0.639749	2.176825	0.068339
-119	2.425216	0.426246	1.690903	0.093214	3.026418	1.345544	1.715783	0.069675
-118	3.120126	0.349313	1.175106	0.094839	1.706509	1.668052	1.24247	0.074026
-117	2.920788	0.230514	0.677708	0.103051	0.024737	1.068064	0.787964	0.082336
-116	2.447714	0.238766	0.242361	0.115711	-0.543645	0.661455	0.393985	0.09818
-115	1.952759	0.247077	-0.12421	0.128941	2.931874	0.500033	0.055779	0.110131
-114	1.499955	0.287105	-0.496744	0.138747	3.010257	0.105825	-0.252917	0.118652
-113	1.23493	0.349524	-0.767707	0.180302	2.631006	0.088928	-0.575059	0.130236
-112	1.260921	0.469448	-0.851807	0.322781	2.228478	0.087884	-0.908776	0.145862
-111	1.11088	0.390681	-0.11843	0.635417	1.840738	0.082389	-0.997165	0.24872
-110	0.912194	0.302194	1.590316	0.524278	1.484668	0.079909	1.395077	0.425708
mean	1.720	0.428	1.439	0.200	1.566	0.435	0.837	0.136